

1

Blind Deconvolution and Structured Matrix Computations with Applications to Array Imaging

Michael K. Ng and Bob Plemmons

Hong Kong Baptist University and Wake Forest University

CONTENTS

1.1	Introduction	1
1.2	One Dimensional Deconvolution Formulation	2
1.3	Regularized and Constrained TLS Formulation	6
1.4	Numerical Algorithms	11
1.5	Two Dimensional Deconvolution Problems	18
1.6	Numerical Examples	21
1.7	Application: High-resolution Image Reconstruction	23
1.8	Concluding Remarks and Current Work	37
	Acknowledgments	39
	References	39

In this chapter, we study using total least squares (TLS) methods for solving blind deconvolution problems arising in image recovery. Here, the true image is to be estimated using only partial information about the blurring operator, or point spread function, which is also subject to error and noise. Iterative, regularized, and constrained TLS methods are discussed and analyzed. As an application, we study TLS methods for the reconstruction of high-resolution images from multiple under sampled images of a scene that is obtained by using a charge-coupled device (CCD) or a CMOS detector array of sensors which are shifted relative to each other by subpixel displacements. The objective is improving the performance of the signal-processing algorithms in the presence of the ubiquitous perturbations of displacements around the ideal subpixel locations because of imperfections in fabrication, etc., or because of shifts designed to enable superresolution reconstructions in array imaging. The target architecture consists of a regular array of identical lenslets whose images are grouped, combined, and then digitally processed. Such a system will have the resolution, field of view, and sensitivity of a camera with an effective aperture that would be considerably larger than the single-lenslet aperture, yet with a short focal length typical of each lenslet. As a means for solving the resulting blind deconvolution problems, the errors-in-variables (or the TLS) method is applied.

1.1 Introduction

The fundamental issue in image enhancement or restoration is blur removal in the presence of observation noise. Recorded images almost always represent a degraded version of the original scene. A primary example is images taken by an optical instrument recording light that has passed through a turbulent medium, such as the atmosphere. Here, changes in the refractive index at different positions in the atmosphere result in a non-planar wavefront [43]. In general, the degradation by noise and blur is caused by fluctuations in both the imaging system and the environment.

In the important case where the blurring operation is *spatially invariant*, the basic restoration computation involved is a deconvolution process that faces the usual difficulties associated with ill-conditioning in the presence of noise [9, Chapter 2]. The image observed from a shift invariant linear blurring process, such as an optical system, is described by how the system blurs a point source of light into a larger image. The image of a point source is called the *point spread function* PSF, which we denote by \mathbf{h} . The observed image \mathbf{g} is then the result of convolving the PSF \mathbf{h} with the “true” image \mathbf{f} , and with noise present in \mathbf{g} .

The *standard deconvolution problem* is to recover the image \mathbf{f} given the observed image \mathbf{g} and the point spread function \mathbf{h} . See, e.g., the survey paper on standard deconvolution written by Banham and Katsaggelos [3]. If the PSF \mathbf{h} is not known, then the problem becomes one of *blind deconvolution*, sometimes called myopic deconvolution if \mathbf{h} is partially known, see, e.g., the survey paper on blind or myopic deconvolution written by Kundar and Hatzinakos [28].

We also mention the recent work of Bardsley, Jefferies, Nagy and Plemmons [4] on the blind restoration of images with an unknown spatially-varying PSF. Their algorithm uses a combination of techniques. First, they section the image, and then treat the sections as a sequence of frames whose unknown PSFs are correlated and approximately spatially-invariant. To estimate the PSFs in each section phase diversity, see, e.g. [49], is used. With these PSF estimates in hand, they then use an interpolation technique to restore the image globally.

In the sections to follow, we concentrate primarily on blind deconvolution. Emphasis is given to the use of TLS methods where the blurring operator has a natural, structured form determined by boundary conditions. Applications to the construction of high-resolution images using low-resolution images from thin array imaging cameras with millimeter diameter lenslets and focal lengths are provided to illustrate the techniques discussed in this chapter.

For a given n , the deconvolution problem is to recover the vector $[f_1, \dots, f_n]^t$ given the point spread function $\bar{\mathbf{h}}$ and a blurred signal $\bar{\mathbf{g}} = [\bar{g}_1, \dots, \bar{g}_n]^t$ of finite length n . Notice that the blurred signal $\bar{\mathbf{g}}$ is determined not only by $\mathbf{f}_c = [f_1, \dots, f_n]^t$, but by $\mathbf{f} = [\mathbf{f}_l \ \mathbf{f}_c \ \mathbf{f}_r]^t$.

The linear system (1.2) is underdetermined. To recover the vector \mathbf{f}_c , we assume the data outside \mathbf{f}_c are reflections of the data inside \mathbf{f}_c , i.e.,

$$\begin{cases} f_0 = f_1 \\ \vdots \\ f_{-n+2} = f_{n-1} \end{cases} \quad \text{and} \quad \begin{cases} f_{n+1} = f_n \\ \vdots \\ f_{2n-1} = f_2. \end{cases} \quad (1.3)$$

In [36], it has been shown that the use of this (Neumann) boundary condition can reduce the boundary artifacts and that solving the resulting systems is much better and faster than using zero and periodic boundary conditions. For example, reverting to the 2-dimensional case for illustration purposes, see Figures 1.1–1.4. The detailed discussion of using the Neumann boundary condition can be found in [36].

In classical image restoration, the point spread function is assumed to be known or adequately sampled [1]. However, in practice, one is often faced with imprecise knowledge of the PSF. For instance, in two dimensional deconvolution problems arising in ground-based atmospheric imaging, the problem consists of an image received by a ground-based imaging system, together with an image of a guide star PSF observed under the effects of atmospheric turbulence. Empirical estimates of the PSF can sometimes be obtained by imaging a relatively bright, isolated point source. The point source might be a natural guide star or a guide star artificially generated using range-gated laser backscatter, e.g., [6, 22, 33]. Notice here that the PSF as well as the image are degraded by blur and noise.

Because the spatial invariance of h translates into the spatial invariance of the noise in the blurring matrix. We assume that the “true” PSF can be represented by the following formula:

$$\bar{\mathbf{h}} = \mathbf{h} + \delta\mathbf{h}, \quad (1.4)$$

where

$$\mathbf{h} = [h_{-n+1}, \dots, h_{n-1}]^t$$

is the estimated (or measured) point spread function and

$$\delta\mathbf{h} = [\delta h_{-n+1}, \delta h_{-n+2}, \dots, \delta h_0, \dots, \delta h_{n-2}, \delta h_{n-1}]^t,$$

is the error component of the PSF. Each δh_i is modeled as independent uniformly distributed noise, with zero-mean and variance σ_h^2 , see for instance [34]. The blurred signal $\bar{\mathbf{g}}$ is also subject to errors. We assume that the observed signal $\mathbf{g} = [g_1, \dots, g_n]^t$ can be represented by

$$\bar{\mathbf{g}} = \mathbf{g} + \delta\mathbf{g}, \quad (1.5)$$

where

$$\delta\mathbf{g} = [\delta g_1, \delta g_2, \dots, \delta g_n]^t$$

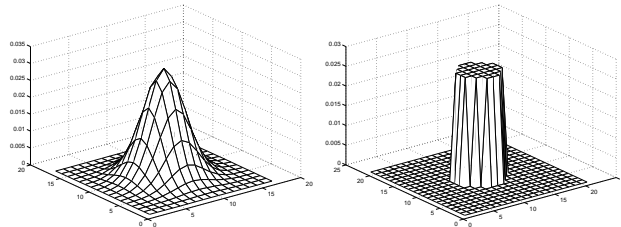


FIGURE 1.1
Gaussian (atmospheric turbulence) blur (left) and out-of-focus blur (right).



FIGURE 1.2
Original image (left), Noisy and blurred satellite image by Gaussian (middle) and out-of-focus blur (right).



rel. error = 1.24×10^{-1} rel. error = 1.15×10^{-1} rel. error = 6.59×10^{-2}

FIGURE 1.3
Restoring Gaussian blur with zero boundary (left), periodic boundary (middle) and Neumann boundary (right) conditions.



rel. error = 1.20×10^{-1} rel. error = 1.09×10^{-1} rel. error = 4.00×10^{-2}

FIGURE 1.4
Restoring out-of-focus blur with zero boundary (left), periodic boundary (middle) and Neumann boundary (right) conditions.

and δg_i is independent uniformly distributed noise with zero-mean and variance σ_g^2 . Here the noise in the PSF and in the observed signal are assumed to be uncorrelated. Thus our image restoration problem is to recover the vector \mathbf{f} from the given inexact point spread function \mathbf{h} and a blurred and noisy signal \mathbf{g} .

1.3 Regularized and Constrained TLS Formulation

In the literature, blind deconvolution methods, see e.g. [12, 25, 28, 39, 40, 50], have been developed to estimate both the true image \mathbf{f} and the point spread function \mathbf{h} from the degraded image \mathbf{g} . In order to obtain a reasonable restored image, these methods require one to impose suitable constraints on the PSF and the image. In our image restoration applications, the PSF is *not* known exactly (e.g., it is corrupted by errors resulting from blur and/or noise). A review of optimization models for blind deconvolution can be found in the survey paper by Kundar and Hatzinakos [28].

Recently there has been growing interest and progress in using total least squares (TLS) methods for solving these blind deconvolution problems arising in image restoration and reconstruction, see e.g., [16, 26, 34, 38, 51, 52]. It is well-known that the total least squares (TLS) is an effective technique for solving a set of error contaminated equations [17, 23]. The TLS method is an appropriate method for consideration in astro-imaging applications. In [26], Kamm and Nagy have proposed the use of the TLS method for solving Toeplitz systems arising from image restoration problems. They applied Newton and Rayleigh quotient iterations to solve the Toeplitz total least squares problems. A possible drawback of their approach is that the point spread function in the TLS formulation is not constrained to be spatially-invariant. Mesarović, Galatsanos and Katsaggelos [34] have shown that formulating the TLS problem for image restoration with the spatially-invariant constraint improves the restored image greatly, see the numerical results in [34].

The determination of \mathbf{f} given the recorded data \mathbf{g} and knowledge of the PSF \mathbf{h} is an inverse problem [15]. Deconvolution algorithms can be extremely sensitive to noise. It is necessary to incorporate regularization into deconvolution to stabilize the computations. Regarding the regularization, Golub, Hansen and O’Leary [16] have shown how Tikhonov regularization methods, for regularized least squares computations, can be recast in a total least squares framework, suited for problems in which both the coefficient matrix and the right-hand side are known only approximately. However, their results do not hold for the constrained total least squares formulation [34]. Therefore, we cannot use the algorithm in [16].

Here we develop constrained TLS approach to solving the image restoration problem, using the one dimensional case for simplicity of presentation.

By using (1.35) and (1.36), the convolution equation (1.2) can be reformulated as follows:

$$H\mathbf{f} - \mathbf{g} + \delta H\mathbf{f} - \delta \mathbf{g} = 0, \quad (1.6)$$

where

$$H = \left[\begin{array}{ccc|ccc} h_{n-1} & \cdots & h_1 & h_0 & \cdots & h_{-n+1} & & 0 \\ & & \ddots & \vdots & & \vdots & & \\ & & & h_{n-1} & & \vdots & h_{-n+1} & \ddots \\ 0 & & & h_{n-1} & \cdots & h_0 & h_{-1} & \cdots & h_{-n+1} \end{array} \right] = [H_l | H_c | H_r] \quad (1.7)$$

and

$$\delta H = \left[\begin{array}{ccc|ccc} \delta h_{n-1} & \cdots & \delta h_1 & \delta h_0 & \cdots & \delta h_{-n+1} & & 0 \\ & & \ddots & \vdots & & \vdots & & \\ & & & \delta h_{n-1} & & \vdots & \delta h_{-n+1} & \ddots \\ 0 & & & \delta h_{n-1} & \cdots & \delta h_0 & \delta h_{-1} & \cdots & \delta h_{-n+1} \end{array} \right] = [\delta H_l | \delta H_c | \delta H_r]. \quad (1.8)$$

Correspondingly, we can define the Toeplitz matrices H_l , H_c and H_r , and δH_l , δH_c and δH_r similar to \bar{H}_l , \bar{H}_c and \bar{H}_r in (1.2), respectively. The constrained total least squares formulation amounts to determining the necessary “minimum” quantities δH and $\delta \mathbf{g}$ such that (1.6) is satisfied.

Mathematically, the constrained total least squares formulation can be expressed as

$$\min_{\mathbf{f}_c} \|[\delta H | \delta \mathbf{g}]\|_F^2 \quad \text{subject to} \quad H\mathbf{f} - \mathbf{g} + \delta H\mathbf{f} - \delta \mathbf{g} = 0,$$

where \mathbf{f} satisfies (1.3).

Recall that image restoration problems are in general ill-conditioned inverse problems and restoration algorithms can be extremely sensitive to noise [18, p.282]. Regularization can be used to achieve stability. Using classical Tikhonov regularization [15, p.117], stability is attained by introducing a regularization operator D and a regularization parameter μ to restrict the set of admissible solutions. More specifically, the regularized solution \mathbf{f}_c is computed as the solution to

$$\min_{\mathbf{f}_c} \{ \|[\delta H | \delta \mathbf{g}]\|_F^2 + \mu \|D\mathbf{f}_c\|_2^2 \} \quad (1.9)$$

subject to

$$H\mathbf{f} - \mathbf{g} + \delta H\mathbf{f} - \delta \mathbf{g} = 0, \quad (1.10)$$

and \mathbf{f} satisfies (1.3). The term $\|D\mathbf{f}_c\|_2^2$ is added in order to regularize the solution. The regularization parameter μ controls the degree of regularity (i.e., degree of bias) of the solution. In many applications [11, 18, 24], $\|D\mathbf{f}_c\|_2$ is chosen to be the L_2 norm $\|\mathbf{f}_c\|_2$ or the H_1 norm $\|L\mathbf{f}_c\|_2$ where L is a first order difference operator matrix. In this paper, we only consider the L_2 and H_1 regularization functionals.

In [34], the authors addressed the problem of restoring images from noisy measurements in both the PSF and the observed data as a regularized and constrained total least squares problem. It was shown in [34] that the regularized minimization problem obtained is nonlinear and nonconvex. Thus fast algorithms for solving this

nonlinear optimization problem are required. In [34], circulant, or periodic, approximations are used to replace the convolution matrices in subsequent computations. In the Fourier domain, the system of nonlinear equations is decoupled into a set of simplified equations and therefore the computational cost can be reduced significantly. However, practical signals and images often do not satisfy these periodic assumptions and ringing effects will appear on the boundary [32]. In the image processing literature, various methods have been proposed to assign boundary values, see Lagendijk and Biemond [29, p.22] and the references therein. For instance, the boundary values may be fixed at a local image mean, or they can be obtained by a model-based extrapolation. In this paper, we consider the image formulation model for the regularized constrained TLS problem using the *Neumann boundary condition* for the image, i.e., we assume that the scene immediately outside is a reflection of the original scene near the boundary. This Neumann boundary condition has been studied in image restoration [29, 32, 36] and in image compression [31, 45]. Results in [36] show that the boundary artifacts resulting from the deconvolution computations are much less prominent than that under the assumption of zero [26] or periodic [34] boundary conditions.

The theorem below characterizes the constrained, regularized TLS formulation of the one dimensional deconvolution problem.

THEOREM 1.1

Under the Neumann boundary condition (1.3), the regularized constrained total least squares solution can be obtained as the \mathbf{f}_c that minimizes the functional:

$$P(\mathbf{f}_c) = (\mathbf{A}\mathbf{f}_c - \mathbf{g})^t \mathbf{Q}(\mathbf{f}_c) (\mathbf{A}\mathbf{f}_c - \mathbf{g}) + \mu \mathbf{f}_c^t \mathbf{D}^t \mathbf{D} \mathbf{f}_c, \quad (1.11)$$

where \mathbf{A} is an n -by- n Toeplitz-plus-Hankel matrix

$$\mathbf{A} = \mathbf{H}_c + [0|\mathbf{H}_l]\mathbf{J} + [\mathbf{H}_r|0]\mathbf{J}, \quad (1.12)$$

\mathbf{J} is the n -by- n reversal matrix,

$$\mathbf{Q}(\mathbf{f}_c) = ([T(\mathbf{f}_c)|I][T(\mathbf{f}_c)|I]^t)^{-1} \equiv [T(\mathbf{f}_c)T(\mathbf{f}_c)^t + I]^{-1},$$

$T(\mathbf{f}_c)$ is an n -by- $(2n-1)$ Toeplitz matrix

$$T(\mathbf{f}_c) = \frac{1}{\sqrt{n}} \begin{bmatrix} f_n & f_{n-1} & \cdots & f_2 & f_1 & f_1 & \cdots & f_{n-2} & f_{n-1} \\ f_n & f_n & \cdots & \cdots & f_2 & f_1 & \cdots & f_{n-3} & f_{n-2} \\ \vdots & \cdots & \cdots & \cdots & \cdots & \cdots & \cdots & \cdots & \vdots \\ f_3 & f_4 & \cdots & f_n & f_{n-1} & \cdots & \cdots & f_1 & f_1 \\ f_2 & f_3 & \cdots & f_n & f_n & f_{n-1} & \cdots & f_2 & f_1 \end{bmatrix}, \quad (1.13)$$

and I is the n -by- n identity matrix.

PROOF From (1.10), we have

$$[T(\mathbf{f}_c)|I] \begin{bmatrix} \sqrt{n}\delta\mathbf{h} \\ -\delta\mathbf{g} \end{bmatrix} = \sqrt{n}T(\mathbf{f}_c)\delta\mathbf{h} - \delta\mathbf{g} = \delta H\mathbf{f} - \delta\mathbf{g} = \mathbf{g} - H\mathbf{f} = \mathbf{g} - A\mathbf{f}_c. \quad (1.14)$$

We note that

$$\|[\delta H|\delta\mathbf{g}]\|_F^2 = n\|\delta\mathbf{h}\|_2^2 + \|\delta\mathbf{g}\|_2^2 = \left\| \begin{bmatrix} \sqrt{n}\delta\mathbf{h} \\ -\delta\mathbf{g} \end{bmatrix} \right\|_2^2.$$

Therefore, we obtain the minimum 2-norm solution of the underdetermined system in (1.14), see for instance [17]. Since the rank of the matrix $[T(\mathbf{f}_c)|I]$ is n , we have

$$\begin{bmatrix} \sqrt{n}\delta\mathbf{h} \\ -\delta\mathbf{g} \end{bmatrix} = [T(\mathbf{f}_c)|I]' Q(\mathbf{f}_c)(\mathbf{g} - A\mathbf{f}_c)$$

or

$$\left\| \begin{bmatrix} \sqrt{n}\delta\mathbf{h} \\ -\delta\mathbf{g} \end{bmatrix} \right\|_2^2 = (A\mathbf{f}_c - \mathbf{g})' Q(\mathbf{f}_c)(A\mathbf{f}_c - \mathbf{g}). \quad (1.15)$$

By inserting (1.15) into (1.9), we obtain (1.11). \blacksquare

1.3.1 Symmetric Point Spread Functions

The estimates of the discrete blurring function may not be unique, in the absence of any additional constraints, mainly because blurs may have any kind of Fourier phase, see [29]. Nonuniqueness of the discrete blurring function can in general be avoided by enforcing a set of constraints. In many papers dealing with blur identification [12, 19, 30], the point spread function is assumed to be symmetric, i.e.,

$$\bar{h}_k = \bar{h}_{-k}, \quad k = 1, 2, \dots, n-1.$$

We remark that point spread functions are often symmetric, see [24, p.269], for instance, the Gaussian point spread function arising in atmospheric turbulence induced blur is symmetric with respect to the origin. For guide star images [19], this is usually not the case. However, they often appear to be fairly symmetric, which can be observed by measuring their distance to a nearest symmetric point spread function. In [19], Hanke and Nagy use the symmetric part of the measured point spread function to restore atmospherically blurred images.

Similarly, we thus incorporate the following symmetry constraints into the total least squares formulation of the problem:

$$\bar{h}_k = \bar{h}_{-k} \quad \text{and} \quad \delta h_k = \delta h_{-k}, \quad k = 1, 2, \dots, n-1. \quad (1.16)$$

Then using Neumann boundary conditions (1.3), the convolution equation (1.6) becomes

$$A\mathbf{f}_c - \mathbf{g} + \delta A\mathbf{f}_c - \delta\mathbf{g} = 0.$$

where A is defined in (1.12) and δA is defined similarly. It was shown in [36] that these Toeplitz-plus-Hankel matrices A and δA can be diagonalized by an n -by- n discrete cosine transform matrix C with entries

$$C_{ij} = \sqrt{\frac{2 - \delta_{i1}}{n}} \cos\left(\frac{(i-1)(2j-1)\pi}{2n}\right), \quad 1 \leq i, j, \leq n,$$

where δ_{ij} is the Kronecker delta, see [24, p.150]. We note that C is orthogonal, i.e., $C^t C = I$. Also, for any n -vector \mathbf{v} , the matrix-vector multiplications $C\mathbf{v}$ and $C^t\mathbf{v}$ can be computed in $O(n \log n)$ real operations by fast cosine transforms (FCTs); see [42, pp.59–60].

In the following discussion, we write

$$A = C^t \text{diag}(\mathbf{w}) C \quad \text{and} \quad \delta A = C^t \text{diag}(\delta \mathbf{w}) C. \quad (1.17)$$

Here for a general vector \mathbf{v} , $\text{diag}(\mathbf{v})$ is a diagonal matrix with its diagonal entries given by

$$[\text{diag}(\mathbf{v})]_{i,i} = \mathbf{v}_i, \quad i = 1, 2, \dots, n.$$

Using (1.17), we can give a new regularized constrained total least squares formulation to this symmetric case as follows:

THEOREM 1.2

Under the Neumann boundary condition (1.3) and the symmetry constraint (1.16), the regularized constrained total least squares solution can be obtained as the $\hat{\mathbf{f}}_c$ that minimizes the functional

$$P(\hat{\mathbf{f}}_c) = [\text{diag}(\mathbf{w})\hat{\mathbf{f}}_c - \hat{\mathbf{g}}]^t \{[\text{diag}(\hat{\mathbf{f}}_c)|I][\text{diag}(\hat{\mathbf{f}}_c)|I]^t\}^{-1} [\text{diag}(\mathbf{w})\hat{\mathbf{f}}_c - \hat{\mathbf{g}}] + \mu \hat{\mathbf{f}}_c^t \Lambda \hat{\mathbf{f}}_c, \quad (1.18)$$

where

$$\hat{\mathbf{f}} = C\mathbf{f}, \quad \hat{\mathbf{g}} = C\mathbf{g},$$

and Λ is an n -by- n diagonal matrix given by

$$\Lambda = CD^t DC^t,$$

and D is the regularization operator.

PROOF In this regularized total least squares formulation, we minimize $\|[\delta A|\delta g]\|_F^2 + \mu \|D\mathbf{f}_c\|_2^2$ subject to $A\mathbf{f}_c - \mathbf{g} + \delta A\mathbf{f}_c - \delta \mathbf{g} = \mathbf{0}$. Since A and δA can be diagonalized by C , the constraint now becomes

$$\text{diag}(\mathbf{w})\hat{\mathbf{f}}_c - \hat{\mathbf{g}} + \text{diag}(\delta \mathbf{w})\hat{\mathbf{f}}_c - \delta \hat{\mathbf{g}} = \mathbf{0}.$$

Let us define $\mathbf{y} = [\text{diag}(\hat{\mathbf{f}}_c)]^{-1} \text{diag}(\delta \mathbf{w})\hat{\mathbf{f}}_c$. It's easy to show that

$$[\text{diag}(\hat{\mathbf{f}}_c)|I] \begin{bmatrix} \mathbf{y} \\ -\delta \hat{\mathbf{g}} \end{bmatrix} = \text{diag}(\hat{\mathbf{f}}_c)\mathbf{y} - \delta \hat{\mathbf{g}} = \text{diag}(\delta \mathbf{w})\hat{\mathbf{f}}_c - \delta \hat{\mathbf{g}} = \hat{\mathbf{g}} - \text{diag}(\mathbf{w})\hat{\mathbf{f}}_c.$$

Hence we have

$$\begin{bmatrix} \mathbf{y} \\ -\delta\hat{\mathbf{g}} \end{bmatrix} = [\text{diag}(\hat{\mathbf{f}}_c)|I]^t \{ [\text{diag}(\hat{\mathbf{f}}_c)|I][\text{diag}(\hat{\mathbf{f}}_c)|I]^t \}^{-1} (\hat{\mathbf{g}} - \text{diag}(\mathbf{w})\hat{\mathbf{f}}_c) \quad (1.19)$$

The diagonalization of A by C implies that

$$\begin{aligned} & \|[\delta A|\delta \mathbf{g}]\|_F^2 \\ &= \|C^t \text{diag}(\delta \mathbf{w})C\|_F^2 + \|C^t \delta \hat{\mathbf{g}}\|_2^2 = \|\text{diag}(\delta \mathbf{w})\|_F^2 + \|\delta \hat{\mathbf{g}}\|_2^2 = \left\| \begin{bmatrix} \mathbf{y} \\ -\delta \hat{\mathbf{g}} \end{bmatrix} \right\|_2^2 \end{aligned}$$

Now, by using (1.19), it's easy to verify that $\|[\delta A|\delta \mathbf{g}]\|_F^2 + \mu \|D\mathbf{f}_c\|_2^2$ is equal to the second member of (1.18). ■

We recall that when the L_2 and H_1 regularization functionals are used in the restoration process, the main diagonal entries of Λ are just given by

$$\Lambda_{ii} = 1 \quad \text{and} \quad \Lambda_{ii} = 4 \cos^2 \left(\frac{(i-1)\pi}{2n} \right), \quad 1 \leq i \leq n,$$

respectively.

1.4 Numerical Algorithms

In this section, we introduce an approach to minimizing (1.11). For simplicity, we let

$$\frac{\partial Q(\mathbf{f}_c)}{\partial f_i} = \begin{bmatrix} \frac{\partial Q_{11}(\mathbf{f}_c)}{\partial f_i} & \dots & \frac{\partial Q_{1n}(\mathbf{f}_c)}{\partial f_i} \\ \vdots & & \vdots \\ \frac{\partial Q_{n1}(\mathbf{f}_c)}{\partial f_i} & \dots & \frac{\partial Q_{nn}(\mathbf{f}_c)}{\partial f_i} \end{bmatrix}.$$

Here $\partial Q_{jk}(\mathbf{f}_c)/\partial f_i$ is the derivative of the (j, k) -th entry of $Q(\mathbf{f}_c)$ with respect to f_i . By applying the product rule to the matrix equality

$$Q(\mathbf{f}_c)[T(\mathbf{f}_c)T(\mathbf{f}_c)^t + I] = I,$$

we obtain

$$\frac{\partial Q(\mathbf{f}_c)}{\partial f_i} = -Q(\mathbf{f}_c) \frac{\partial \{T(\mathbf{f}_c)T(\mathbf{f}_c)^t + I\}}{\partial f_i} Q(\mathbf{f}_c)$$

or equivalently

$$\frac{\partial Q(\mathbf{f}_c)}{\partial f_i} = -Q(\mathbf{f}_c) \left\{ \frac{\partial T(\mathbf{f}_c)}{\partial f_i} T(\mathbf{f}_c)^t + T(\mathbf{f}_c) \frac{\partial T(\mathbf{f}_c)^t}{\partial f_i} \right\} Q(\mathbf{f}_c).$$

The gradient $G(\mathbf{f}_c)$ (derivative with respect to \mathbf{f}_c) of the functional (1.11) is given by

$$G(\mathbf{f}_c) = 2A^t Q(\mathbf{f}_c)(A\mathbf{f}_c - \mathbf{g}) + 2\mu D^t D\mathbf{f}_c + \mathbf{u}(\mathbf{f}_c),$$

where

$$\mathbf{u}(\mathbf{f}_c) = \begin{bmatrix} (A\mathbf{f}_c - \mathbf{g})^t \frac{\partial Q(\mathbf{f}_c)}{\partial f_1} (A\mathbf{f}_c - \mathbf{g}) \\ (A\mathbf{f}_c - \mathbf{g})^t \frac{\partial Q(\mathbf{f}_c)}{\partial f_2} (A\mathbf{f}_c - \mathbf{g}) \\ \vdots \\ (A\mathbf{f}_c - \mathbf{g})^t \frac{\partial Q(\mathbf{f}_c)}{\partial f_n} (A\mathbf{f}_c - \mathbf{g}) \end{bmatrix}.$$

The gradient descent scheme, yields

$$\mathbf{f}_c^{(k+1)} = \mathbf{f}_c^{(k)} - \tau_k G(\mathbf{f}_c^{(k)}), \quad k = 0, 1, \dots.$$

A line search can be added to select the step size τ_k in a manner which gives sufficient decrease in the objective functional in (1.11) to guarantee convergence to a minimizer. This gives the method of steepest descent, see [14, 27, 35]. While numerical implementation is straightforward, steepest descent has rather undesirable asymptotic convergence properties which can make it very inefficient. Obviously, one can apply other standard unconstrained optimization methods with better convergence properties, like the nonlinear conjugate gradient method or Newton's method. These methods converge rapidly near a minimizer provided the objective functional depends smoothly on \mathbf{f}_c . Since the objective function in (1.11) is nonconvex, this results in a loss of robustness and efficiency for higher order methods like Newton's method. Moreover, implementing Newton's method requires the inversion of an n -by- n unconstructed matrix, clearly an overwhelming task for any reasonable-sized image, for instance, $n = 65,536$ for a 256×256 image. Thus, these approaches may all be unsuitable for the image restoration problem.

Here we develop an alternative approach to minimizing (1.11). At a minimizer, we know that $G(\mathbf{f}_c) = 0$, or equivalently,

$$2A^t Q(\mathbf{f}_c)(A\mathbf{f}_c - \mathbf{g}) + 2\mu D^t D\mathbf{f}_c - \mathbf{u}(\mathbf{f}_c) = 0.$$

The iteration can be expressed as

$$\left[A^t Q(\mathbf{f}_c^{(k)})A + \mu D^t D \right] \mathbf{f}_c^{(k+1)} = \frac{\mathbf{u}(\mathbf{f}_c^{(k)})}{2} + A^t Q(\mathbf{f}_c^{(k)})\mathbf{g}. \quad (1.20)$$

Note that at each iteration, one must solve a linear system depending on the previous iterate $\mathbf{f}_c^{(k)}$, to obtain the new iterate $\mathbf{f}_c^{(k+1)}$. We also find that

$$\mathbf{d}^{(k)} = \mathbf{f}_c^{(k+1)} - \mathbf{f}_c^{(k)} = -\frac{1}{2} \left[A^t Q(\mathbf{f}_c^{(k)})A + \mu D^t D \right]^{-1} G(\mathbf{f}_c^{(k)}).$$

Hence the iteration is of quasi-Newton form, and existing convergence theory can be applied, see for instance [14, 27]. Since the matrix $Q(\mathbf{f}_c^{(k)})$ is symmetric positive

definite, and therefore $(A^t Q(\mathbf{f}_c^{(k)})A + \mu D^t D)$ is symmetric positive definite with its eigenvalues bounded away from zero (because of the regularization), each step computes the descent direction $\mathbf{d}^{(k)}$, and global convergence can be guaranteed by using the appropriate step size, i.e.,

$$\mathbf{f}_c^{(k+1)} = \mathbf{f}_c^{(k)} - \frac{\tau_k}{2} \left[A^t Q(\mathbf{f}_c^{(k)})A + \mu D^t D \right]^{-1} G(\mathbf{f}_c^{(k)}),$$

where

$$\tau_k = \operatorname{argmin}_{\tau^k > 0} P(\mathbf{f}_c^{(k)} + \tau^k \mathbf{d}^{(k)}).$$

With this proposed iterative scheme, one must solve a symmetric positive definite linear system

$$\left[A^t Q(\mathbf{f}_c^{(k)})A + \mu D^t D \right] \mathbf{x} = \mathbf{b} \quad (1.21)$$

for some \mathbf{b} at each iteration. Of course these systems are dense in general, but have structures that can be utilized. We apply a preconditioned conjugate gradient method to solving these linear systems.

1.4.1 The Preconditioned Conjugate Gradient Method

In this subsection, we introduce the conjugate gradient method for solving linear systems of equations. For a more in-depth treatment of other Krylov space methods see [44]. The CG method was invented in the 1950s [21] (Hestenes and Steifel, 1952) as a direct method for solving Hermitian positive definite systems. It has come into wide use over the last 20 years as an iterative method.

Let us consider $A\mathbf{x} = \mathbf{b}$ where $A \in \mathbb{C}^{n \times n}$ is a nonsingular Hermitian positive definite matrix and $\mathbf{b} \in \mathbb{C}^n$. Given an initial guess \mathbf{x}_0 and the corresponding initial residual $\mathbf{r}_0 = \mathbf{b} - A\mathbf{x}_0$, the k th iterate \mathbf{x}_k of CG minimizes the functional

$$\phi(\mathbf{x}) \equiv \frac{1}{2} \mathbf{x}^* A \mathbf{x} - \mathbf{x}^* \mathbf{b}$$

over $\mathbf{x}_0 + \mathcal{K}_k$, where \mathcal{K}_k is the k th Krylov subspace

$$\mathcal{K}_k \equiv \operatorname{span}(\mathbf{r}_0, A\mathbf{r}_0, \dots, A^{k-1}\mathbf{r}_0), \quad k = 1, 2, \dots$$

Note that if \mathbf{x} minimizes $\phi(\mathbf{x})$, then $\nabla \phi(\mathbf{x}) = A\mathbf{x} - \mathbf{b} = 0$ and hence \mathbf{x} is the solution.

Denote \mathbf{x}_t , the true solution of the system, and define the norm

$$\|\mathbf{x}\|_A \equiv \sqrt{\mathbf{x}^* A \mathbf{x}}.$$

One can show that minimizing $\phi(\mathbf{x})$ over $\mathbf{x}_0 + \mathcal{K}_k$ is the same as minimizing $\|\mathbf{x} - \mathbf{x}_t\|_A$ over $\mathbf{x}_0 + \mathcal{K}_k$, i.e.

$$\|\mathbf{x}_t - \mathbf{x}_k\|_A = \min_{\mathbf{y} \in \mathbf{x}_0 + \mathcal{K}_k} \|\mathbf{x}_t - \mathbf{y}\|_A.$$

Since any $\mathbf{y} \in \mathbf{x}_0 + \mathcal{H}_k$ can be written as

$$\mathbf{y} = \mathbf{x}_0 + \sum_{i=0}^{k-1} \alpha_i A^i \mathbf{r}_0$$

for some coefficients $\{\alpha_i\}_{i=0}^{k-1}$, we can express $\mathbf{x}_t - \mathbf{y}$ as

$$\mathbf{x}_t - \mathbf{y} = \mathbf{x}_t - \mathbf{x}_0 - \sum_{i=0}^{k-1} \alpha_i A^i \mathbf{r}_0.$$

As $\mathbf{r}_0 = \mathbf{b} - A\mathbf{x}_0 = A(\mathbf{x}_t - \mathbf{x}_0)$, we have

$$\mathbf{x}_t - \mathbf{y} = \mathbf{x}_t - \mathbf{x}_0 - \sum_{i=0}^{k-1} \alpha_i A^{i+1} (\mathbf{x}_t - \mathbf{x}_0) = p(A)(\mathbf{x}_t - \mathbf{x}_0),$$

where the polynomial

$$p(z) = 1 - \sum_{i=0}^{k-1} \alpha_i z^{i+1}$$

has degree k and satisfies $p(0) = 1$. Hence

$$\|\mathbf{x}_t - \mathbf{x}_k\|_A = \min_{p \in \mathcal{P}_k, p(0)=1} \|p(A)(\mathbf{x}_t - \mathbf{x}_0)\|_A, \quad (1.22)$$

where \mathcal{P}_k is the set of polynomials of degree k .

Hermitian positive definite matrices asserts that $A = U\Lambda U^*$, where U is a unitary matrix whose columns are the eigenvectors of A and Λ is the diagonal matrix with the positive eigenvalues of A on the diagonal. Since $UU^* = U^*U = I$, we have $A^k = U\Lambda^k U^*$. Hence $p(A) = Up(\Lambda)U^*$. Defining $A^{\frac{1}{2}} = U\Lambda^{\frac{1}{2}}U^*$, we have

$$\|p(A)\mathbf{x}\|_A = \|A^{\frac{1}{2}}p(A)\mathbf{x}\|_2 \leq \|p(A)\|_2 \|\mathbf{x}\|_A.$$

Together with (1.22), this implies that

$$\|\mathbf{x}_t - \mathbf{x}_k\|_A \leq \|\mathbf{x}_t - \mathbf{x}_0\|_A \min_{p \in \mathcal{P}_k, p(0)=1} \max_{\lambda \in \sigma(A)} |p(\lambda)|. \quad (1.23)$$

Clearly, if $k = n$, we can choose p to be the n th-degree polynomial that passes through all the eigenvalues $\lambda \in \sigma(A)$ with $p(0) = 1$. Then the maximum in the right-hand side of (1.23) is zero and we have the following theorem in Axelsson and Barker [2, p.24].

THEOREM 1.3

Let A be a Hermitian positive definite matrix of size n . Then the CG algorithm finds the solution of $A\mathbf{x} = \mathbf{b}$ within n iterations in the absence of roundoff errors.

In most applications, the number of unknowns n is very large. It is better to consider CG as an iterative method and terminate the iteration when some specified error tolerance is reached. The usual implementation of the CG method is to find, for a given ε , a vector \mathbf{x} such that $\|\mathbf{b} - \mathbf{A}\mathbf{x}\|_2 \leq \varepsilon\|\mathbf{b}\|_2$. Algorithm CG is a typical implementation of the method. Its inputs are the right-hand side \mathbf{b} , a routine which computes the action of A on a vector, and the initial guess \mathbf{x}_0 which will be overwritten by the subsequent iterates \mathbf{x}_k . We limit the number of iterations to k_{\max} and return the solution \mathbf{x}_k and the residual norm ρ_k .

Algorithm CG($\mathbf{x}, \mathbf{b}, A, \varepsilon, k_{\max}$)

1. $\mathbf{r} = \mathbf{b} - \mathbf{A}\mathbf{x}$, $\rho_0 = \|\mathbf{r}\|_2^2$, $k = 1$
2. Do while $\sqrt{\rho_{k-1}} > \varepsilon\|\mathbf{b}\|_2$ and $k < k_{\max}$
 - if $k = 1$ then $\mathbf{p} = \mathbf{r}$
 - else
 - $\beta = \rho_{k-1}/\rho_{k-2}$ and $\mathbf{p} = \mathbf{r} + \beta\mathbf{p}$
 - $\mathbf{w} = \mathbf{A}\mathbf{p}$
 - $\alpha = \rho_{k-1}/\mathbf{p}^*\mathbf{w}$
 - $\mathbf{x} = \mathbf{x} + \alpha\mathbf{p}$
 - $\mathbf{r} = \mathbf{r} - \alpha\mathbf{w}$
 - $\rho_k = \|\mathbf{r}\|_2^2$
 - $k = k + 1$
3. End Do

Note that the matrix A itself need not be formed or stored — only a routine for matrix–vector products $\mathbf{A}\mathbf{p}$ is required.

Next we consider the cost. We need to store only four vectors: \mathbf{x} , \mathbf{w} , \mathbf{p} , and \mathbf{r} . Each iteration requires a single matrix–vector product to compute $\mathbf{w} = \mathbf{A}\mathbf{p}$, two scalar products (one for $\mathbf{p}^*\mathbf{w}$ and one to compute $\rho_k = \|\mathbf{r}\|_2^2$), and three operations of the form $\alpha\mathbf{x} + \mathbf{y}$, where \mathbf{x} and \mathbf{y} are vectors and α is a scalar. Thus, besides the matrix–vector multiplication, each iteration of Algorithm CG requires $O(n)$ operations*, where n is the size of the matrix A .

The convergence rate of the conjugate gradient method can be determined by the condition number $\kappa(A)$ of the matrix A , where

$$\kappa(A) \equiv \|A\|_2 \cdot \|A^{-1}\|_2 = \frac{\lambda_{\max}(A)}{\lambda_{\min}(A)}.$$

*Let f and g be two functions defined on the set of integers. We say that $f(n) = O(g(n))$ as $n \rightarrow \infty$ if there exists a constant K such that $|f(n)/g(n)| \leq K$ as $n \rightarrow \infty$.

In fact, by choosing p in (1.23) to be a k th degree Chebyshev polynomial, one can derive the following theorem in Axelsson and Barker [2, p.26].

THEOREM 1.4

Let A be a Hermitian positive definite matrix with condition number $\kappa(A)$. Then the k th iterate \mathbf{x}_k of the conjugate gradient method satisfies

$$\frac{\|\mathbf{x}_t - \mathbf{x}_k\|_A}{\|\mathbf{x}_t - \mathbf{x}_0\|_A} \leq 2 \left(\frac{\sqrt{\kappa(A)} - 1}{\sqrt{\kappa(A)} + 1} \right)^k. \quad (1.24)$$

In particular, for any given tolerance $\tau > 0$, $\|\mathbf{x}_t - \mathbf{x}_k\|_A / \|\mathbf{x}_t - \mathbf{x}_0\|_A \leq \tau$ if

$$k \geq \frac{1}{2} \sqrt{\kappa(A)} \log \left(\frac{2}{\tau} \right) + 1 = O(\sqrt{\kappa(A)}). \quad (1.25)$$

This shows that the convergence rate is linear:

$$\frac{\|\mathbf{x}_t - \mathbf{x}_k\|_A}{\|\mathbf{x}_t - \mathbf{x}_0\|_A} \leq 2r^k$$

where $r < 1$. However, if we have more information about the spectrum of A , then we can have a better bound of the error as the following theorem asserts (cf. also Axelsson (1994)).

When the condition number or the distribution of the eigenvalues of a matrix is not good, one can improve the performance of the CG iteration by preconditioning. In effect, one tries to replace the given system $A\mathbf{x} = \mathbf{b}$ by another Hermitian positive definite system with the same solution \mathbf{x} , but with the new coefficient matrix having a more favorable spectrum.

Suppose that P is a Hermitian positive definite matrix such that either the condition number of $P^{-1}A$ is close to 1 or the eigenvalues of $P^{-1}A$ are clustered around 1. Then, the CG method, when applied to the preconditioned system

$$P^{-1}A\mathbf{x} = P^{-1}\mathbf{b},$$

will converge very fast. We will call P the *preconditioner* of the system $A\mathbf{x} = \mathbf{b}$ or of the matrix A . The following algorithm is a typical implementation of the preconditioned conjugate gradient (PCG) method. The input of this algorithm is the same as that for Algorithm CG, except that we now have an extra routine to compute the action of the inverse of the preconditioner on a vector.

Algorithm PCG($\mathbf{x}, \mathbf{b}, A, P, \varepsilon, k_{\max}$)

1. $\mathbf{r} = \mathbf{b} - A\mathbf{x}$, $\rho_0 = \|\mathbf{r}\|_2^2$, $k = 1$
2. Do while $\sqrt{\rho_{k-1}} > \varepsilon \|\mathbf{b}\|_2$ and $k < k_{\max}$
 - $\mathbf{z} = P^{-1}\mathbf{r}$ (or solve $P\mathbf{z} = \mathbf{r}$)

```

 $\tau_{k-1} = \mathbf{z}^* \mathbf{r}$ 
if  $k = 1$  then  $\beta = 0$  and  $\mathbf{p} = \mathbf{z}$ 
else
 $\beta = \tau_{k-1} / \tau_{k-2}$  and  $\mathbf{p} = \mathbf{z} + \beta \mathbf{p}$ 
 $\mathbf{w} = A\mathbf{p}$ 
 $\alpha = \tau_{k-1} / \mathbf{p}^* \mathbf{w}$ 
 $\mathbf{x} = \mathbf{x} + \alpha \mathbf{p}$ 
 $\mathbf{r} = \mathbf{r} - \alpha \mathbf{w}$ 
 $\rho_k = \|\mathbf{r}\|_2^2$ 
 $k = k + 1$ 

```

3. End Do

Note that the cost of Algorithm PCG is identical to that of Algorithm CG with the addition of the solution of the preconditioner system $P\mathbf{z} = \mathbf{r}$ and the inner product to compute τ_{k-1} in Step 2. Thus the criteria for choosing a good preconditioner P are:

- The system $P\mathbf{z} = \mathbf{r}$ for any given \mathbf{r} should be solved efficiently.
- The spectrum of $P^{-1}A$ should be clustered and/or its condition number should be close to 1.

1.4.2 Cosine Transform Based Preconditioners

In this application, we need to compute a matrix-vector product

$$(A^t Q(\mathbf{f}_c^{(k)}) A + \mu D^t D) \mathbf{v}$$

for some vector \mathbf{v} in each CG iteration. Since the matrices A and A^t are Toeplitz-plus-Hankel matrices, their matrix-vector multiplications can be done in $O(n \log n)$ operations for any n -vector, see for instance [10]. However, for the matrix-vector product

$$Q(\mathbf{f}_c^{(k)}) \mathbf{v} \equiv \{ [T(\mathbf{f}_c^{(k)}) | I] [T(\mathbf{f}_c^{(k)}) | I]^t \}^{-1} \mathbf{v},$$

we need to solve another linear system

$$\left\{ [T(\mathbf{f}_c^{(k)}) | I] [T(\mathbf{f}_c^{(k)}) | I]^t \right\} \mathbf{z} = \mathbf{v}. \quad (1.26)$$

Notice that the matrix-vector multiplications $T(\mathbf{f}_c^{(k)}) \mathbf{y}$ and $T(\mathbf{f}_c^{(k)})^t \mathbf{v}$ can also be computed $O(n \log n)$ operations for any n -vector \mathbf{y} . A preconditioned conjugate gradient method will also be used for solving this symmetric positive definite linear system.

We remark that all matrices that can be diagonalized by the discrete cosine transform matrix C must be symmetric [36], so C above can only diagonalize matrices

with symmetric point spread functions for this problem. On the other hand, for nonsymmetric point spread functions, we can construct cosine transform based preconditioners to speed up the convergence of the conjugate gradient method.

Given a matrix X , we define the optimal cosine transform preconditioner $c(X)$ to be the minimizer of $\|X - Q\|_F^2$ over all Q that can be diagonalized by C , see [36]. In this case, the cosine transform preconditioner $c(A)$ of A in (1.12) is defined to be the matrix $C^t \Lambda C$ such that Λ minimizes

$$\|C^t \Lambda C - A\|_F^2.$$

Here Λ is any nonsingular diagonal matrix. Clearly, the cost of computing $c(A)^{-1}\mathbf{y}$ for any n -vector \mathbf{y} is $O(n \log n)$ operations. In [36], Ng et al. gave a simple approach for finding $c(A)$. The cosine transform preconditioner $c(A)$ is just the blurring matrix (cf. (1.12)) corresponding to the symmetric point spread function $s_i \equiv (h_i + h_{-i})/2$ with the Neumann boundary condition imposed. This approach allows us to precondition the symmetric positive definite linear system (1.21).

Next we construct the cosine transform preconditioner for $\{[T(\mathbf{f}_c^{(k)})|I][T(\mathbf{f}_c^{(k)})|I]^t\}$ which exploits the Toeplitz structure of the matrix. We approximate $T(\mathbf{f}_c)$ by

$$\tilde{T}(\mathbf{f}_c) = \frac{1}{2n-1} \begin{bmatrix} f_n & f_{n-1} & \cdots & f_2 & f_1 & 0 & \cdots & \cdots & 0 \\ 0 & f_n & \ddots & \ddots & f_2 & f_1 & \ddots & & 0 \\ \vdots & \ddots & \ddots & \ddots & \ddots & \ddots & \ddots & \ddots & \vdots \\ 0 & & \ddots & f_n & f_{n-1} & \ddots & \ddots & f_1 & 0 \\ 0 & \cdots & \cdots & 0 & f_n & f_{n-1} & \cdots & f_2 & f_1 \end{bmatrix}$$

In [37], Ng and Plemmons have proved that if \mathbf{f}_c is a stationary stochastic process, then the expected value of $T(\mathbf{f}_c)T(\mathbf{f}_c)^t - \tilde{T}(\mathbf{f}_c)\tilde{T}(\mathbf{f}_c)^t$ is close to zero. Since $\tilde{T}(\mathbf{f}_c)\tilde{T}(\mathbf{f}_c)^t$ is a Toeplitz matrix, $c(\tilde{T}(\mathbf{f}_c)\tilde{T}(\mathbf{f}_c)^t)$ can be found in $O(n)$ operations, see [10]. However, the original matrix $T(\mathbf{f}_c)T(\mathbf{f}_c)^t$ is much more complicated and thus the construction cost of $c(\tilde{T}(\mathbf{f}_c)\tilde{T}(\mathbf{f}_c)^t)$ is cheaper than that of $c(T(\mathbf{f}_c)T(\mathbf{f}_c)^t)$. It is clear that the cost of computing $c(\tilde{T}(\mathbf{f}_c)\tilde{T}(\mathbf{f}_c)^t)^{-1}\mathbf{y}$ for any n -vector \mathbf{y} is again $O(n \log n)$ operations. It follows that the cost per each iteration in solving the linear systems (1.21) and (1.26) are $O(n \log n)$ operations.

Finally, we remark that the objective function is simplified in the cosine transform domain when the symmetry constraints are incorporated into the total least squares formulation. In accordance with the Theorem 2, the minimization of $P(\hat{\mathbf{f}}_c)$ in (1.18) is equivalent to

$$\min_{\hat{\mathbf{f}}_i} \left[\frac{(\mathbf{w}_i \hat{\mathbf{f}}_i - \hat{\mathbf{g}}_i)^2}{\hat{\mathbf{f}}_i^2 + 1} + \mu \Lambda_{ii} \hat{\mathbf{f}}_i^2 \right], \quad 1 \leq i \leq n.$$

We note that the objective function is decoupled into n equations, each to be minimized independently with respect to one DCT coefficient of $\hat{\mathbf{f}}_c$. It follows that each minimizer can be determined by an one-dimensional search method, see [35].

1.5 Two Dimensional Deconvolution Problems

The results of the previous section extend in a natural way to two dimensional image deconvolution. The main interest concerns optical image enhancement. Applications of image deconvolution in optics can be found in many areas of science and engineering, e.g., see the book by Roggemann and Welsh [43]. For example, work to enhance the quality of optical images has important applications in astronomical imaging [22]. Only partial priori knowledge about the degradation phenomena or point spread function in aero-optics is generally known, so here the use of constrained total least squares method is appropriate. In addition, the estimated point spread function is generally degraded in a manner similar to that of the observed image [43].

Let $f(x,y)$ and $\bar{g}(x,y)$ be the functions of the original and the blurred images respectively. The image restoration problem can be expressed as a linear integral equation

$$\bar{g}(x,y) = \int \int \bar{h}(x-y, u-v) f(y,v) dy dv. \quad (1.27)$$

The convolution operation, as is often the case in optical imaging, acts uniformly (i.e., in a spatially invariant manner) on f . We consider numerical methods for approximating the solution to the linear restoration problem in discretized (matrix) form obtained from (1.27). For notation purposes we assume that the image is n -by- n , and thus contains n^2 pixels. Typically, n is chosen to be a power of 2, such as 256 or larger. Then the number of unknowns grows to at least 65,536. The vectors \mathbf{f} and $\bar{\mathbf{g}}$ represent the “true” and observed image pixel values, respectively, unstacked by rows. After discretization of (1.27), the blurring matrix \bar{H} defined by \bar{h} is given by

$$\bar{H} = \left[\begin{array}{ccc|ccc} H^{(n-1)} & \dots & H^{(1)} & H^{(0)} & \dots & H^{(-n+1)} & & 0 \\ & & \ddots & \vdots & & \vdots & H^{(-n+1)} & \\ & & & \vdots & & \vdots & & \ddots \\ & & & H^{(n-1)} & & \vdots & & \\ 0 & & & H^{(n-1)} & \dots & H^{(0)} & H^{(-1)} & \dots & H^{(-n+1)} \end{array} \right] \quad (1.28)$$

with each subblock $H^{(j)}$ being a n -by- $(2n-1)$ matrix of the form given by (1.7). The dimensions of the discrete point spread function h are $2n-1$ and $2n-1$ in the x -direction and y -direction, respectively.

Applying Neumann boundary conditions, the resulting matrix A is a block-Toeplitz-

plus-Hankel matrix with Toeplitz-plus-Hankel blocks. More precisely,

$$A = \begin{bmatrix} A^{(0)} & A^{(-1)} & \dots & \dots & A^{(-n+1)} \\ A^{(1)} & A^{(0)} & \ddots & \ddots & \vdots \\ \vdots & \ddots & \ddots & \ddots & \vdots \\ \vdots & \ddots & \ddots & A^{(0)} & A^{(-1)} \\ A^{(n-1)} & \dots & \dots & A^{(1)} & A^{(0)} \end{bmatrix} + \begin{bmatrix} A^{(1)} & A^{(2)} & \dots & A^{(n-1)} & 0 \\ A^{(2)} & & \ddots & \ddots & A^{(-n+1)} \\ \vdots & \ddots & \ddots & \ddots & \vdots \\ A^{(n-1)} & \ddots & \ddots & & A^{(-2)} \\ 0 & A^{(-n+1)} & \dots & A^{(-2)} & A^{(-1)} \end{bmatrix} \quad (1.29)$$

with each block $A^{(j)}$ being an n -by- n matrix of the form given in (1.12). We note that the $A^{(j)}$ in (1.29) and the $H^{(j)}$ in (1.28) are related by (1.12). A detailed discussion of using the Neumann boundary conditions for two dimensional problems can be found in [36].

Using a similar argument, we can formulate the regularized constrained total least squares problems under the Neumann boundary conditions.

THEOREM 1.5

Under the Neumann boundary condition (1.3), the regularized constrained total least squares solution can be obtained as the \mathbf{f}_c that minimizes the functional:

$$P(\mathbf{f}_c) = (\mathbf{A}\mathbf{f}_c - \mathbf{g})^t ([T|I][T|I]^t)^{-1} (\mathbf{A}\mathbf{f}_c - \mathbf{g}) + \mu \mathbf{f}_c^t D^t D \mathbf{f}_c,$$

where T is an n^2 -by- $(2n-1)^2$ block-Toeplitz-Toeplitz-block matrix

$$T = \frac{1}{n} \begin{bmatrix} T_n & T_{n-1} & \dots & T_2 & T_1 & T_1 & \dots & T_{n-2} & T_{n-1} \\ T_n & T_n & \ddots & \ddots & T_2 & T_1 & \ddots & T_{n-3} & T_{n-2} \\ \vdots & \ddots & \ddots & \ddots & \ddots & \ddots & \ddots & \ddots & \vdots \\ T_3 & T_4 & \ddots & T_n & T_{n-1} & \ddots & \ddots & T_1 & T_1 \\ T_2 & T_3 & \dots & T_n & T_n & T_{n-1} & \dots & T_2 & T_1 \end{bmatrix}$$

and each subblock T_j is a n -by- $(2n-1)$ matrix of the form given by (1.7).

For a symmetric point spread function, we have the following theorem.

THEOREM 1.6

Under the Neumann boundary condition (1.3) and the symmetry constraint

$$h_{i,j} = h_{i,-j} = h_{-i,j} = h_{-i,-j},$$

the regularized constrained total least squares solution can be obtained as the $\hat{\mathbf{f}}_c$ that minimizes the functional

$$P(\mathbf{f}_c) = [\text{diag}(\mathbf{w})\hat{\mathbf{f}}_c - \hat{\mathbf{g}}]^t \{ [\text{diag}(\hat{\mathbf{f}}_c)|I][\text{diag}(\hat{\mathbf{f}}_c)|I]^t \}^{-1} [\text{diag}(\mathbf{w})\hat{\mathbf{f}}_c - \hat{\mathbf{g}}] + \mu \hat{\mathbf{f}}_c^t \Lambda \hat{\mathbf{f}}_c,$$



FIGURE 1.5
“Gatlinburg Conference” test image.

where $\hat{\mathbf{f}} = \mathbf{C}\mathbf{f}$, $\hat{\mathbf{g}} = \mathbf{C}\mathbf{g}$, and Λ is an n -by- n diagonal matrix given by $\Lambda = \mathbf{C}\mathbf{D}'\mathbf{D}\mathbf{C}'$ and \mathbf{D} is the regularization operator.

1.6 Numerical Examples

In this section, we illustrate that the quality of restored image given by using the regularized, constrained TLS method with the Neumann boundary conditions is generally superior to that obtained by the least squares method. The data source is a photo from the 1964 Gatlinburg Conference on Numerical Algebra taken from Matlab. From (1.2), we see that to construct the right hand side vector $\hat{\mathbf{g}}$ correctly, we need the vectors \mathbf{f}_l and \mathbf{f}_r , i.e., we need to know the image outside the given domain. Thus we start with the 480-by-640 image of the photo and cut out a 256-by-256 portion from the image. Figure 1.5 gives the 256-by-256 image of this picture.

We consider restoring the “Gatlinburg Conference” image blurred by a truncated (band limited) Gaussian point spread function,

$$h_{i,j} = \begin{cases} ce^{-0.1(i^2+j^2)}, & \text{if } |i-j| \leq 8, \\ 0, & \text{otherwise,} \end{cases}$$

see [24, p.269]., where $h_{i,j}$ is the j th entry of the first column of $A^{(i)}$ in (1.29) and c is the normalization constant such that $\sum_{i,j} h_{i,j} = 1$. We remark that the Gaussian point spread function is symmetric, and is often used in the literature to simulate the blurring effects of imaging through the atmosphere [3, 43]. Gaussian noise with signal-to-noise ratios of 40dB, 30dB and 20dB is then added to the blurred images and the point spread functions to produce test images. Noisy, blurred images are

Blurred image Noise added SNR (dB)	PSF Noise added SNR (dB)	Exact PSF RLS method	Noisy PSF RLS method	Noisy PSF RCTLS method
40	20	7.78×10^{-2}	1.07×10^{-1}	8.94×10^{-2}
40	30	7.78×10^{-2}	8.72×10^{-2}	8.48×10^{-2}
40	40	7.78×10^{-2}	8.07×10^{-2}	8.03×10^{-2}
30	20	8.66×10^{-2}	1.07×10^{-1}	9.98×10^{-2}
30	30	8.66×10^{-2}	9.17×10^{-2}	8.88×10^{-2}
30	40	8.66×10^{-2}	8.75×10^{-2}	8.71×10^{-2}
20	20	9.68×10^{-2}	1.13×10^{-1}	1.09×10^{-1}
20	30	9.68×10^{-2}	1.00×10^{-1}	9.99×10^{-2}
20	40	9.68×10^{-2}	9.76×10^{-2}	9.77×10^{-2}

Table 1.1: The relative errors for different methods.

shown in Figures 1.6(a). We note that after the blurring, the cigarette held by Prof. Householder (the rightmost person) is not clearly shown.

In Table 1.1, we present results for the regularized constrained total least squares method with PSF symmetry constraints. We denote this method by RCTLS in the table. As a comparison, the results in solving the regularized least squares (RLS) problems with the exact and noisy point spread functions are also listed. For all methods tested, the Neumann boundary conditions are employed and the corresponding blurring matrices can be diagonalized by discrete cosine transform matrix. Therefore, the image restoration can be done efficiently in the transform domain. We remark that Tikhonov regularization of the least squares method can be recast as in a total least squares framework, see [16]. In the tests, we used the L_2 norm as the regularization functional. The corresponding regularization parameters μ are chosen to minimize the relative error of the restored image which is defined as

$$\frac{\|\mathbf{f}_c - \mathbf{f}_c(\mu)\|_2}{\|\mathbf{f}_c\|_2}, \quad (1.30)$$

where \mathbf{f}_c is the original image. In the tests, the regularization parameters are obtained by trial and error.

We see from Table 1.1 that the relative errors in using the RCTLS method are less than that of using RLS method with the noisy PSF, except the case where the SNR of noises added to the blurred image and PSF are 20dB and 40dB respectively. However, for some cases, the improvement of using RCTLS method is not significant when the SNR ratio is low, that is, the noise level to the blurred image is very high. In Figure 1.6, we present the restored images for different methods. We see from Figure 1.6 that the cigarette is better restored by using the RCTLS method than that by using the RLS method. We remark that the corresponding relative error is also significantly smaller than that obtained by using the RLS method. When noise with low SNR is added to the blurred image and point spread function, visually, the restored images look similar. In Figure 1.6(e), we present the restored images for the

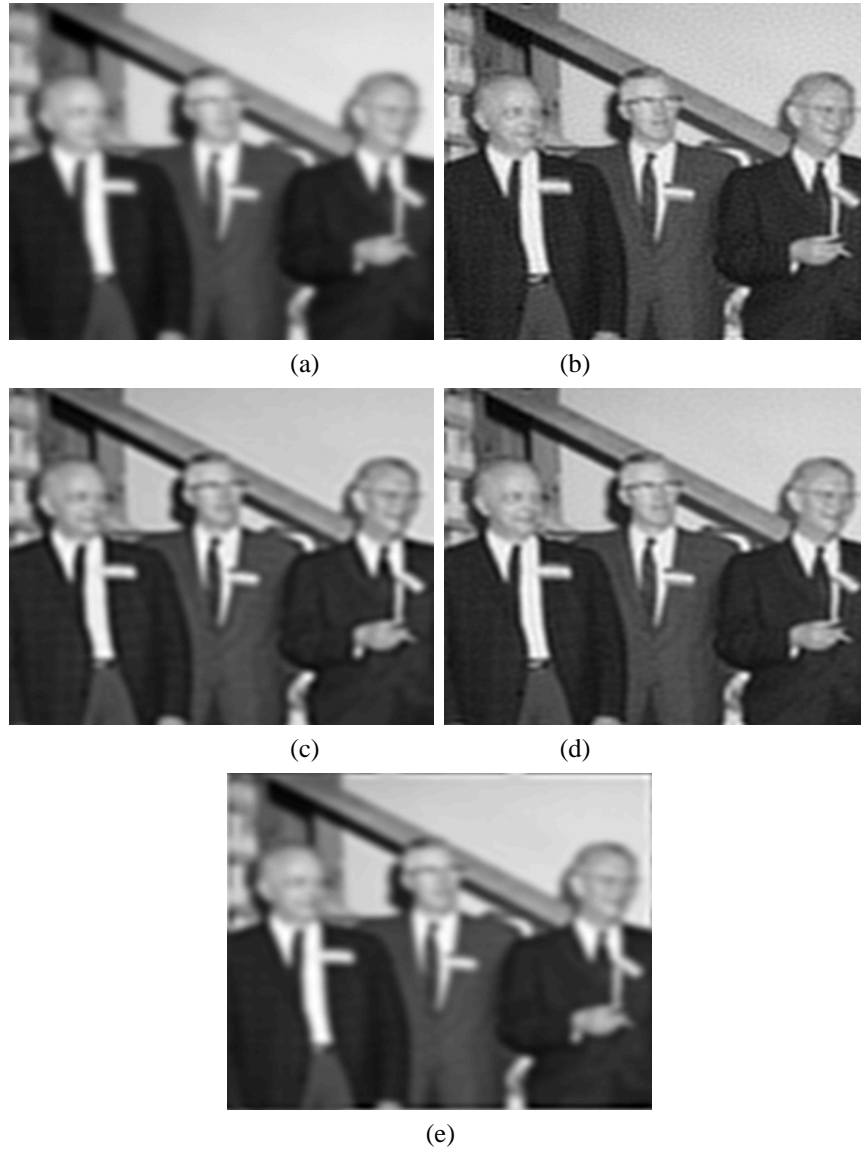
periodic boundary condition using the RCTLS method. We see from all the figures that by using the RCTLS method and imposing the Neumann boundary condition, the relative errors and the ringing effects in the restorations are significantly reduced.

1.7 Application: High-resolution Image Reconstruction

Processing methods for single images often provide unacceptable results because of the ill-conditioned nature of associated inverse problems and the lack of diversity in the data. Therefore, image processing using a sequence of images, as well as images captured simultaneously using a camera with multiple lenslets, has developed into an active research area because multiple deconvolution operators can be used to make the problem better posed. Rapid progress in computer and semiconductor technology is making it possible to implement such image processing tasks reasonably quickly, but the need for processing in real time requires attention to design of efficient and robust algorithms for implementation on current and future generations of computational architectures.

Image sequences may be produced from several snapshots of an object or a scene (LANDSAT images). Using sequential estimation theory in the wave number domain, an efficient method was developed [8] for interpolating and recursively updating to provide filtering provided the displacements of the frames with respect to a reference frame were either known or estimated. It was observed that the performance deteriorated when the blur produced zeros in the wave number domain and theoretical justification for this can be provided. The problem of reconstruction in the wave number domain with errors present both in the observation and data was tackled by the total least squares method [48].

The spatial resolution of an image is often determined by imaging sensors. In a CCD or a CMOS camera, the image resolution is determined by the size of its photo-detector. An ensemble of several shifted images could be collected by a pre-fabricated planar array of CCD or CMOS sensors and one may reconstruct with higher resolution which is equivalent to an effective increase of the sampling rate by interpolation. Fabrication limitations are known to cause subpixel displacement errors, which coupled with observation noise limit the deployment of least squares techniques in this scenario. TLS is an effective technique for solving a set of such error contaminated equations [48] and therefore is an appropriate method for consideration in high-resolution image reconstruction applications. However, a possible drawback of using the conventional TLS approach is that the formulation is not constrained to handle point spread functions obtained from multisensors. In this section, an image processing technique that leads to the deployment of constrained total least squares (CTLS) theory is described. Then a computational procedure is advanced and the role of regularization is considered.

**FIGURE 1.6**

(a) Noisy and blurred images with SNR of 40dB, the restored images by using (b) the exact PSF (rel. err. = 7.78×10^{-2}), (c) the RLS method for the noisy PSF with SNR of 20dB (rel. err. = 1.07×10^{-1}), (d) the RCTLS method for a noisy PSF with SNR of 20dB under Neumann boundary conditions (rel. err. = 8.94×10^{-2}) and (e) the RCTLS method for a noisy PSF with SNR of 20dB under periodic boundary conditions (rel. err. = 1.14×10^{-1}).

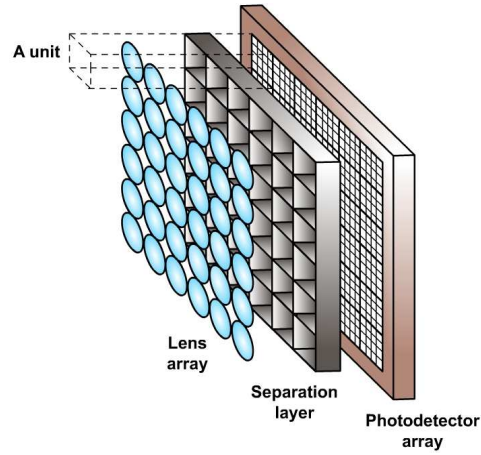


FIGURE 1.7
A depiction of the basic components of an array imaging camera system [46].

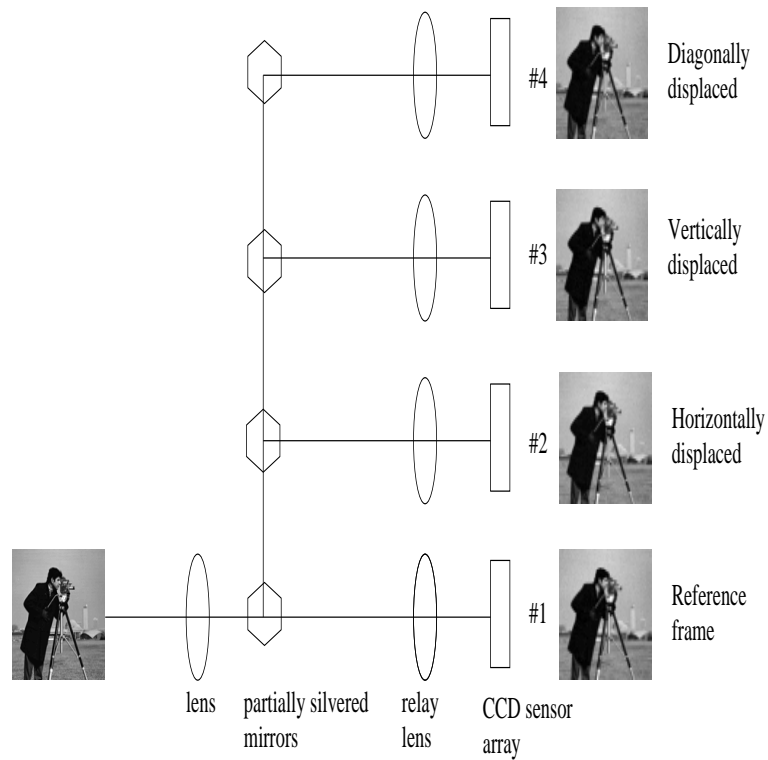


FIGURE 1.8
Example of low-resolution image formation.

1.7.1 Mathematical Model

A brief introduction to a mathematical model in high-resolution image reconstruction is provided first, see Figure 1.9. Details can be found in [7]. Consider a sensor array with $L_1 \times L_2$ sensors in which each sensor has $N_1 \times N_2$ sensing elements (pixels) and the size of each sensing element is $T_1 \times T_2$. The goal is to reconstruct an image of resolution $M_1 \times M_2$, where $M_1 = L_1 N_1$ and $M_2 = L_2 N_2$. To maintain the aspect ratio of the reconstructed image the case where $L_1 = L_2 = L$ is considered. For simplicity, L is assumed to be an even positive integer in the following discussion.

To generate enough information to resolve the high-resolution image, subpixel displacements between sensors are necessary. In the ideal case, the sensors are shifted from each other by a value proportional to $T_1/L \times T_2/L$. However, in practice there can be small perturbations around these ideal subpixel locations due to imperfections of the mechanical imaging system during fabrication. Thus, for $l_1, l_2 = 0, 1, \dots, L-1$ with $(l_1, l_2) \neq (0, 0)$, the horizontal and vertical displacements $d_{l_1 l_2}^x$ and $d_{l_1 l_2}^y$, respectively, of the $[l_1, l_2]$ -th sensor with respect to the $[0, 0]$ -th reference sensor are given by

$$d_{l_1 l_2}^x = \frac{T_1}{L}(l_1 + \bar{\epsilon}_{l_1 l_2}^x) \quad \text{and} \quad d_{l_1 l_2}^y = \frac{T_2}{L}(l_2 + \bar{\epsilon}_{l_1 l_2}^y),$$

where $\bar{\epsilon}_{l_1 l_2}^x$ and $\bar{\epsilon}_{l_1 l_2}^y$ denote, respectively, the actual normalized horizontal and vertical displacement errors. The estimates, $\epsilon_{l_1 l_2}^x$ and $\epsilon_{l_1 l_2}^y$, of these parameters, $\bar{\epsilon}_{l_1 l_2}^x$ and $\bar{\epsilon}_{l_1 l_2}^y$, can be obtained by manufacturers during camera calibration.

It is reasonable to assume that

$$|\bar{\epsilon}_{l_1 l_2}^x| < \frac{1}{2} \quad \text{and} \quad |\bar{\epsilon}_{l_1 l_2}^y| < \frac{1}{2},$$

because if that is not the case, then the low-resolution images acquired from two different sensors may have more than the desirable overlapping information for reconstructing satisfactorily the high-resolution image [7].

Let $f(x_1, x_2)$ denote the original bandlimited high-resolution scene, as a function of the continuous spatial variables, x_1, x_2 . Then the observed low-resolution digital image $\bar{g}_{l_1 l_2}$ acquired from the (l_1, l_2) -th sensor, characterized by a point-spread function, is modeled by

$$\bar{g}_{l_1 l_2}[n_1, n_2] = \int_{T_2(n_2 - \frac{1}{2}) + d_{l_1 l_2}^y}^{T_2(n_2 + \frac{1}{2}) + d_{l_1 l_2}^y} \int_{T_1(n_1 - \frac{1}{2}) + d_{l_1 l_2}^x}^{T_1(n_1 + \frac{1}{2}) + d_{l_1 l_2}^x} f(x_1, x_2) dx_1 dx_2, \quad (1.31)$$

for $n_1 = 1, \dots, N_1$ and $n_2 = 1, \dots, N_2$. These low-resolution images are combined to yield the $M_1 \times M_2$ high-resolution image \bar{g} by assigning its pixel values according to

$$\bar{g}[L(n_1 - 1) + l_1, L(n_2 - 1) + l_2] = \bar{g}_{l_1 l_2}[n_1, n_2], \quad (1.32)$$

for $l_1, l_2 = 0, 1, \dots, (L-1)$, $n_1 = 1, \dots, N_1$ and $n_2 = 1, \dots, N_2$.

The continuous image model $f(x_1, x_2)$ in (1.31) can be discretized by the rectangular rule and approximated by a discrete image model. Let \mathbf{g} and \mathbf{f} be, respectively, the

vectors formed from discretization of $g(x_1, x_2)$ and $f(x_1, x_2)$ using a column ordering. The Neumann boundary condition is applied on the images. This assumes that the scene immediately outside is a reflection of the original scene at the boundary, i.e.,

$$f(i, j) = f(k, l) \quad \text{where} \quad \begin{cases} k = 1 - i, & i < 1, \\ k = 2M_1 + 1 - i, & i > M_1, \\ l = 1 - j, & j < 1, \\ l = 2M_2 + 1 - j, & j > M_2. \end{cases}$$

Under the Neumann boundary condition, the blurring matrices are banded matrices with bandwidth $L + 1$, but the entries at the upper left part and the lower right part of the matrices are changed. The resulting matrices, denoted by $H_{l_1 l_2}^x(\bar{\epsilon}_{l_1, l_2}^x)$ and $H_{l_1 l_2}^y(\bar{\epsilon}_{l_1, l_2}^y)$, have a Toeplitz-plus-Hankel structure.

$$H_{l_1 l_2}^x(\bar{\epsilon}_{l_1, l_2}^x) = \frac{1}{L} \begin{pmatrix} \overbrace{1 \quad \cdots \quad 1}^{L/2 \text{ ones}} & \frac{1}{2} - \bar{\epsilon}_{l_1 l_2}^x & 0 \\ \vdots & \ddots & \ddots \\ 1 & \ddots & \ddots & \frac{1}{2} - \bar{\epsilon}_{l_1 l_2}^x \\ \frac{1}{2} + \bar{\epsilon}_{l_1 l_2}^x & \ddots & \ddots & 1 \\ 0 & \ddots & \ddots & \vdots \\ 0 & \frac{1}{2} + \bar{\epsilon}_{l_1 l_2}^x & 1 & \cdots & 1 \end{pmatrix} + \frac{1}{L} \begin{pmatrix} \overbrace{1 \quad \cdots \quad 1}^{L/2-1 \text{ ones}} & \frac{1}{2} + \bar{\epsilon}_{l_1 l_2}^x & 0 \\ \vdots & \ddots & \ddots \\ 1 & \ddots & \ddots & \frac{1}{2} - \bar{\epsilon}_{l_1 l_2}^x \\ \frac{1}{2} + \bar{\epsilon}_{l_1 l_2}^x & \ddots & \ddots & 1 \\ 0 & \frac{1}{2} - \bar{\epsilon}_{l_1 l_2}^x & 1 & \cdots & 1 \end{pmatrix}. \quad (1.33)$$

The matrix $H_{l_1 l_2}^y(\bar{\epsilon}_{l_1, l_2}^y)$ is defined similarly. The blurring matrix corresponding to the (l_1, l_2) -th sensor under the Neumann boundary condition is given by the Kronecker product,

$$H_{l_1 l_2}(\bar{\epsilon}_{l_1, l_2}) = H_{l_1 l_2}^x(\bar{\epsilon}_{l_1, l_2}^x) \otimes H_{l_1 l_2}^y(\bar{\epsilon}_{l_1, l_2}^y),$$

where the 2×1 vector $\bar{\epsilon}_{l_1, l_2}$ is denoted by $(\bar{\epsilon}_{l_1, l_2}^x \quad \bar{\epsilon}_{l_1, l_2}^y)^t$. The blurring matrix for the

whole sensor array is made up of blurring matrices from each sensor:

$$H_L(\bar{\mathbf{e}}) = \sum_{l_1=0}^{L-1} \sum_{l_2=0}^{L-1} D_{l_1 l_2} H_{l_1 l_2}(\bar{\mathbf{e}}_{l_1, l_2}), \quad (1.34)$$

where the $2L^2 \times 1$ vector $\bar{\mathbf{e}}$ is defined as

$$\bar{\mathbf{e}} = [\bar{\mathbf{e}}_{00}^x \ \bar{\mathbf{e}}_{00}^y \ \bar{\mathbf{e}}_{01}^x \ \bar{\mathbf{e}}_{01}^y \ \cdots \ \bar{\mathbf{e}}_{L-1L-2}^x \ \bar{\mathbf{e}}_{L-1L-2}^y \ \bar{\mathbf{e}}_{L-1L-1}^x \ \bar{\mathbf{e}}_{L-1L-1}^y]^t.$$

Here $D_{l_1 l_2}$ are diagonal matrices with diagonal elements equal to 1 if the corresponding component of \mathbf{g} comes from the (l_1, l_2) -th sensor and zero otherwise, see [7] for more details.

1.7.2 Image Reconstruction Formulation

In this subsection, the displacement errors are not known exactly. The spatial invariance of the blurring function translates into the spatial invariance of the displacement error in the blurring matrix. The ‘‘true’’ blur function is represented as follows. For each $l_1, l_2 \in \{0, 1, \dots, L-1\}$,

$$\bar{\mathbf{h}}_{l_1 l_2}^z = \frac{1}{L} \overbrace{\left[\frac{1}{2} - \bar{\mathbf{e}}_{l_1 l_2}^z \quad 1 \cdots 1 \cdots 1 \quad \frac{1}{2} + \bar{\mathbf{e}}_{l_1 l_2}^z \right]^t}^{\text{there are } L+1 \text{ entries}} = \mathbf{h}_{l_1 l_2}^z + \delta \mathbf{h}_{l_1 l_2}^z, \quad \forall z \in \{x, y\}, \quad (1.35)$$

where the $(L+1) \times 1$ component vectors are

$$\mathbf{h}_{l_1 l_2}^z = \frac{1}{L} \left[\frac{1}{2} - \mathbf{e}_{l_1 l_2}^z \quad 1 \cdots 1 \cdots 1 \quad \frac{1}{2} + \mathbf{e}_{l_1 l_2}^z \right]^t, \quad z \in \{x, y\}$$

and

$$\delta \mathbf{h}_{l_1 l_2}^z = \frac{1}{L} [-\delta \mathbf{e}_{l_1 l_2}^z \quad 0 \cdots 0 \cdots 0 \quad \delta \mathbf{e}_{l_1 l_2}^z]^t, \quad z \in \{x, y\}.$$

Here $\mathbf{h}_{l_1 l_2}^z$ is the estimated (or measured) point spread function and $\delta \mathbf{h}_{l_1 l_2}^z$ is the error component of the point spread function at the (l_1, l_2) th sensor in the z -direction ($z \in \{x, y\}$).

The observed signal vector $\bar{\mathbf{g}}$ is also subject to errors. It is assumed that this observed $M_1 M_2 \times 1$ signal vector $\bar{\mathbf{g}} = [g_1 \ \dots \ g_{M_1 M_2}]^t$ can be represented by

$$\bar{\mathbf{g}} = \mathbf{g} + \delta \mathbf{g}, \quad (1.36)$$

where

$$\delta \mathbf{g} = [\delta g_1 \ \delta g_2 \ \cdots \ \delta g_{M_1 M_2}]^t$$

and $\{\delta g_i\}$ is independent and identically distributed Gaussian noise with zero mean and variance σ_g^2 . Then the image reconstruction problem requires the recovery of the vector \mathbf{f} from the given inexact point spread function function $\mathbf{h}_{l_1 l_2}^z$ ($l_1 = 0, 1, \dots, L_1 - 1, l_2 = 0, 1, \dots, L_2 - 1, z \in \{x, y\}$) and the observed noisy signal vector $\bar{\mathbf{g}}$.

The constrained TLS formulation for multisensors is considered. Using

$$H_L(\bar{\boldsymbol{\varepsilon}})\mathbf{f} = \sum_{l_1=0}^{L-1} \sum_{l_2=0}^{L-1} D_{l_1 l_2} H_{l_1 l_2}(\bar{\boldsymbol{\varepsilon}}_{l_1, l_2})\mathbf{f} = \bar{\mathbf{g}} = \mathbf{g} + \boldsymbol{\delta}\mathbf{g}$$

(from (1.34)) and (1.35) and (1.36), the preceding equation can be reformulated as follows:

$$\begin{aligned} & \left[\sum_{l_1=0}^{L-1} \sum_{l_2=0}^{L-1} D_{l_1 l_2} \left(H_{l_1 l_2}^x(\boldsymbol{\varepsilon}_{l_1, l_2}) \otimes H_{l_1 l_2}^y(\boldsymbol{\varepsilon}_{l_1, l_2}) \right) \right] \mathbf{f} - \mathbf{g} + \\ & \left[\sum_{l_1=0}^{L-1} \sum_{l_2=0}^{L-1} \delta \boldsymbol{\varepsilon}_{l_1 l_2}^x \left(D_{l_1 l_2} E \otimes H_{l_1 l_2}^y(\boldsymbol{\varepsilon}_{l_1, l_2}) \right) \right] \mathbf{f} \\ & \left[\sum_{l_1=0}^{L-1} \sum_{l_2=0}^{L-1} \delta \boldsymbol{\varepsilon}_{l_1 l_2}^y \left(D_{l_1 l_2} H_{l_1 l_2}^x(\boldsymbol{\varepsilon}_{l_1, l_2}) \otimes E \right) \right] \mathbf{f} + \\ & \left[\sum_{l_1=0}^{L-1} \sum_{l_2=0}^{L-1} \delta \boldsymbol{\varepsilon}_{l_1 l_2}^x \delta \boldsymbol{\varepsilon}_{l_1 l_2}^y \left(D_{l_1 l_2} E \otimes E \right) \right] \mathbf{f} - \boldsymbol{\delta}\mathbf{g} = 0 \end{aligned}$$

or

$$\begin{aligned} & \left[\sum_{l_1=0}^{L-1} \sum_{l_2=0}^{L-1} D_{l_1 l_2} \left(H_{l_1 l_2}^x(\boldsymbol{\varepsilon}_{l_1, l_2}) \otimes H_{l_1 l_2}^y(\boldsymbol{\varepsilon}_{l_1, l_2}) \right) \right] \mathbf{f} - \mathbf{g} + \sum_{l_1=0}^{L-1} \sum_{l_2=0}^{L-1} \delta \boldsymbol{\varepsilon}_{l_1 l_2}^x \mathbf{f}_{l_1 l_2}^y \\ & \sum_{l_1=0}^{L-1} \sum_{l_2=0}^{L-1} \delta \boldsymbol{\varepsilon}_{l_1 l_2}^y \mathbf{f}_{l_1 l_2}^x + \left[\sum_{l_1=0}^{L-1} \sum_{l_2=0}^{L-1} \delta \boldsymbol{\varepsilon}_{l_1 l_2}^x \delta \boldsymbol{\varepsilon}_{l_1 l_2}^y \left(D_{l_1 l_2} E \otimes E \right) \right] \mathbf{f} - \boldsymbol{\delta}\mathbf{g} = 0, \quad (1.37) \end{aligned}$$

where

$$E = \frac{1}{L} \begin{pmatrix} \overbrace{0 \cdots 0}^{L/2 \text{ zeros}} & -1 & & 0 \\ \vdots & \ddots & \ddots & \vdots \\ 0 & \cdots & \cdots & -1 \\ 1 & \cdots & \cdots & 0 \\ \vdots & \ddots & \ddots & \vdots \\ 0 & 1 & 0 & \cdots & 0 \end{pmatrix} + \frac{1}{L} \begin{pmatrix} \overbrace{0 \cdots 0}^{L/2-1 \text{ zeros}} & 1 & & 0 \\ \vdots & \ddots & \ddots & \vdots \\ 0 & \cdots & \cdots & -1 \\ 1 & \cdots & \cdots & 0 \\ \vdots & \ddots & \ddots & \vdots \\ 0 & -1 & 0 & \cdots & 0 \end{pmatrix}$$

$\underbrace{\hspace{10em}}_{L/2 \text{ zeros}} \qquad \underbrace{\hspace{10em}}_{L/2-1 \text{ zeros}}$

and

$$\mathbf{f}_{l_1 l_2}^x = D_{l_1 l_2} \left(H_{l_1 l_2}^x(\boldsymbol{\varepsilon}_{l_1, l_2}) \otimes E \right) \mathbf{f}, \quad \mathbf{f}_{l_1 l_2}^y = D_{l_1 l_2} \left(E \otimes H_{l_1 l_2}^y(\boldsymbol{\varepsilon}_{l_1, l_2}) \right) \mathbf{f}.$$

The constrained TLS formulation amounts to minimizing the norms of vectors associated with

$$\{\delta\boldsymbol{\varepsilon}_{l_1 l_2}^x, \delta\boldsymbol{\varepsilon}_{l_1 l_2}^y\}_{l_1, l_2=0}^{L-1} \quad \text{and} \quad \delta\mathbf{g}$$

as explained below such that (1.37) is satisfied.

However, it is first noted that because $\delta\boldsymbol{\varepsilon}_{l_1 l_2}^z$ ($l_1, l_2 = 0, 1, \dots, L-1$) should be very small, the quantity $|\delta\boldsymbol{\varepsilon}_{l_1 l_2}^x \delta\boldsymbol{\varepsilon}_{l_1 l_2}^y|$ can be assumed to be negligible, and, therefore, the nonlinear term

$$\left[\sum_{l_1=0}^{L-1} \sum_{l_2=0}^{L-1} \delta\boldsymbol{\varepsilon}_{l_1 l_2}^x \delta\boldsymbol{\varepsilon}_{l_1 l_2}^y (D_{l_1 l_2} E \otimes E) \right] \mathbf{f} \quad (1.38)$$

can be ignored in (1.37). In this case, (1.37) reduces to a linear system involving $\{\delta\boldsymbol{\varepsilon}_{l_1 l_2}^x, \delta\boldsymbol{\varepsilon}_{l_1 l_2}^y\}_{l_1, l_2=0}^{L-1}$ and $\delta\mathbf{g}$.

For simplicity, denote the $2L^2 \times 1$ vector

$$\Delta = [\delta\boldsymbol{\varepsilon}_{00}^x \delta\boldsymbol{\varepsilon}_{00}^y \delta\boldsymbol{\varepsilon}_{01}^x \delta\boldsymbol{\varepsilon}_{01}^y \cdots \delta\boldsymbol{\varepsilon}_{L-1L-2}^x \delta\boldsymbol{\varepsilon}_{L-1L-2}^y \delta\boldsymbol{\varepsilon}_{L-1L-1}^x \delta\boldsymbol{\varepsilon}_{L-1L-1}^y]^t.$$

Mathematically, the constrained TLS formulation can be expressed as

$$\min_{\mathbf{f}} \left\| \begin{bmatrix} \Delta \\ \delta\mathbf{g} \end{bmatrix} \right\|_2^2$$

subject to

$$H_L(\boldsymbol{\varepsilon})\mathbf{f} - \mathbf{g} + \sum_{l_1=0}^{L-1} \sum_{l_2=0}^{L-1} \delta\boldsymbol{\varepsilon}_{l_1 l_2}^x \cdot \mathbf{f}_{l_1 l_2}^y + \sum_{l_1=0}^{L-1} \sum_{l_2=0}^{L-1} \delta\boldsymbol{\varepsilon}_{l_1 l_2}^y \cdot \mathbf{f}_{l_1 l_2}^x - \delta\mathbf{g} = 0 \quad (1.39)$$

Image reconstruction problems are in general ill-conditioned inverse problems and reconstruction algorithms can be extremely sensitive to noise [18]. Regularization can be used to achieve stability. Using classical Tikhonov regularization [15], stability is attained by introducing a regularization operator P and a regularization parameter μ to restrict the set of admissible solutions. More specifically, the regularized solution \mathbf{f} is computed as the solution to

$$\min_{\mathbf{f}} \left\| \begin{bmatrix} \Delta \\ \delta\mathbf{g} \end{bmatrix} \right\|_2^2 + \mu \|P\mathbf{f}\|_2^2 \quad (1.40)$$

subject to (1.39). The term $\mu \|P\mathbf{f}\|_2^2$ is added in order to regularize the solution. The regularization parameter μ controls the degree of regularity (i.e., degree of bias) of the solution. In many applications [18, 24], $\|P\mathbf{f}\|_2$ is chosen to be $\|\mathbf{f}\|_2$ or $\|R\mathbf{f}\|_2$ where R is a first order difference operator matrix.

The theorem below characterizes the regularized, constrained total least squares (RCTLS) formulation of the high-resolution reconstruction problem with multisensors.

THEOREM 1.7

The regularized constrained total least squares solution can be obtained as the \mathbf{f} that minimizes the functional:

$$J(\mathbf{f}) = (H_L(\varepsilon)\mathbf{f} - \mathbf{g})^t \{ [Q(\mathbf{f}) | -\mathbf{I}_{M_1 M_2}] [Q(\mathbf{f}) | -\mathbf{I}_{M_1 M_2}]^t \}^{-1} (H_L(\varepsilon)\mathbf{f} - \mathbf{g}) + \mu \mathbf{f}^t P^t P \mathbf{f}, \quad (1.41)$$

$$Q(\mathbf{f}) = [\mathbf{f}_{00}^y | \mathbf{f}_{00}^x | \mathbf{f}_{01}^y | \mathbf{f}_{01}^x | \cdots | \mathbf{f}_{L-1L-2}^y | \mathbf{f}_{L-1L-2}^x | \mathbf{f}_{L-1L-1}^y | \mathbf{f}_{L-1L-1}^x].$$

and $\mathbf{I}_{M_1 M_2}$ is the $M_1 M_2$ -by- $M_1 M_2$ identity matrix.

The proof of the above theorem is similar to Theorems 1.1 and 1.5. The resulting objective function (1.41) to be minimized is nonconvex and nonlinear. In the next section, an iterative algorithm that takes advantage, computationally, of the fast solvers for image reconstruction problems with known displacement errors [7, 41] is developed.

By (1.39) and (1.40),

$$\begin{aligned} \min_{\mathbf{f}, \Delta} J(\mathbf{f}, \Delta) \equiv \min_{\mathbf{f}, \Delta} \{ & \|\Delta\|_2^2 + \\ & \left\| H_L(\varepsilon)\mathbf{f} - \mathbf{g} + \sum_{l_1=0}^{L-1} \sum_{l_2=0}^{L-1} \delta \varepsilon_{l_1 l_2}^x \cdot \mathbf{f}_{l_1 l_2}^y + \sum_{l_1=0}^{L-1} \sum_{l_2=0}^{L-1} \delta \varepsilon_{l_1 l_2}^y \cdot \mathbf{f}_{l_1 l_2}^x \right\|_2^2 + \mu \|P\mathbf{f}\|_2^2 \} \end{aligned} \quad (1.42)$$

It is noted that the above objective function is equivalent to (1.41).

Before solving for \mathbf{f} in the RCTLS formulation, it is first noted that for a given \mathbf{f} , the function $J(\mathbf{f}, \cdot)$ is convex with respect to Δ , and for a given Δ , the function $J(\cdot, \Delta)$ is also convex with respect to \mathbf{f} . Therefore, with an initial guess Δ_0 , one can minimize (1.42) by first solving

$$J(\mathbf{f}_1, \Delta_0) \equiv \min_{\mathbf{f}} J(\cdot, \Delta_0)$$

and then

$$J(\mathbf{f}_1, \Delta_1) \equiv \min_{\Delta} J(\mathbf{f}_1, \cdot).$$

Therefore, an alternating minimization algorithm is developed in which the function value $J(\mathbf{f}_n, \Delta_n)$ always decreases as n increases. More precisely, the algorithm is stated as follows:

Assume that Δ_{n-1} is available:

- Determine \mathbf{f}_n by solving the following least squares problem

$$\min_{\mathbf{f}_n} \left\{ \left\| H_L(\varepsilon)\mathbf{f}_n - \mathbf{g} + \sum_{l_1=0}^{L-1} \sum_{l_2=0}^{L-1} \delta \varepsilon_{n-1 l_1 l_2}^x \mathbf{f}_n^y + \sum_{l_1=0}^{L-1} \sum_{l_2=0}^{L-1} \delta \varepsilon_{n-1 l_1 l_2}^y \mathbf{f}_n^x \right\|_2^2 + \mu \|P\mathbf{f}_n\|_2^2 \right\} \quad (1.43)$$

Here,

$$\mathbf{f}_{n \ l_1 l_2}^x = D_{l_1 l_2} (H_{l_1 l_2}^x(\boldsymbol{\varepsilon}_{l_1, l_2}) \otimes E) \mathbf{f}_n \quad \text{and} \quad \mathbf{f}_{n \ l_1 l_2}^y = D_{l_1 l_2} (E \otimes H_{l_1 l_2}^y(\boldsymbol{\varepsilon}_{l_1, l_2})) \mathbf{f}_n. \quad (1.44)$$

As we have noted that the nonlinear term (1.38) can be assumed to be negligible, we can add this term in the objective function (1.43). Therefore, the least squares solution \mathbf{f}_n can be found by solving the following linear system:

$$[H_L(\boldsymbol{\varepsilon} + \Delta_{n-1})^t H_L(\boldsymbol{\varepsilon} + \Delta_{n-1}) + \mu P^t P] \mathbf{f}_n = H_L(\boldsymbol{\varepsilon} + \Delta_{n-1})^t \mathbf{g}. \quad (1.45)$$

- Determine Δ_n by solving the following least squares problem

$$\min_{\Delta_n} \left\{ \|\Delta_n\|_2^2 + \left\| H_L(\boldsymbol{\varepsilon}) \mathbf{f}_n - \mathbf{g} + \sum_{l_1=0}^{L-1} \sum_{l_2=0}^{L-1} \delta \boldsymbol{\varepsilon}_{l_1 l_2}^x \mathbf{f}_{n \ l_1 l_2}^y + \sum_{l_1=0}^{L-1} \sum_{l_2=0}^{L-1} \delta \boldsymbol{\varepsilon}_{l_1 l_2}^y \mathbf{f}_{n \ l_1 l_2}^x \right\|_2^2 \right\}. \quad (1.46)$$

Using (1.44) and (1.41), the above equation can be rewritten as

$$\min_{\Delta_n} \left\{ \|\Delta_n\|_2^2 + \|H_L(\boldsymbol{\varepsilon}) \mathbf{f}_n - \mathbf{g} + Q(\mathbf{f}_n) \Delta_n\|_2^2 \right\}, \quad (1.47)$$

where $Q_n(\mathbf{f})$ is defined as in Theorem 1.7. The cost function in (1.47) becomes

$$\begin{aligned} J(f_n, \Delta_n) &= \Delta_n^t \Delta_n + (H_L(\boldsymbol{\varepsilon}) \mathbf{f}_n - \mathbf{g} + Q(\mathbf{f}_n) \Delta_n)^t (H_L(\boldsymbol{\varepsilon}) \mathbf{f}_n - \mathbf{g} + Q(\mathbf{f}_n) \Delta_n) \\ &= \Delta_n^t \Delta_n + (H_L(\boldsymbol{\varepsilon}) \mathbf{f}_n - \mathbf{g})^t (H_L(\boldsymbol{\varepsilon}) \mathbf{f}_n - \mathbf{g}) + (H_L(\boldsymbol{\varepsilon}) \mathbf{f}_n - \mathbf{g})^t Q(\mathbf{f}_n) \Delta_n + \\ &\quad (Q(\mathbf{f}_n) \Delta_n)^t (H_L(\boldsymbol{\varepsilon}) \mathbf{f}_n - \mathbf{g}) + (Q(\mathbf{f}_n) \Delta_n)^t (Q(\mathbf{f}_n) \Delta_n). \end{aligned}$$

Here \mathbf{f}_n is fixed. The gradient of this cost function with respect to Δ_n is equal to

$$2 \Delta_n + 2Q(\mathbf{f}_n)^t (H_L(\boldsymbol{\varepsilon}) \mathbf{f}_n - \mathbf{g}) + 2Q(\mathbf{f}_n)^t Q(\mathbf{f}_n) \Delta_n,$$

and therefore the minimum 2-norm least squares solution Δ_n is given by

$$\Delta_n = [\mathbf{I}_{2L^2} + Q(\mathbf{f}_n)^t Q(\mathbf{f}_n)]^{-1} Q(\mathbf{f}_n)^t (\mathbf{g} - H_L(\boldsymbol{\varepsilon}) \mathbf{f}_n). \quad (1.48)$$

The costly stage in the algorithm is the inversion of the matrix

$$H_L(\boldsymbol{\varepsilon} + \Delta_{n-1})^t H_L(\boldsymbol{\varepsilon} + \Delta_{n-1}) + \mu P^t P.$$

The preconditioned conjugate gradient method can be applied to solve the linear system

$$\begin{aligned} & [c(H_L(\boldsymbol{\varepsilon} + \Delta_{n-1}))^t c(H_L(\boldsymbol{\varepsilon} + \Delta_{n-1})) + \mu c(P^t P)]^{-1} \\ & [H_L(\boldsymbol{\varepsilon} + \Delta_{n-1})^t H_L(\boldsymbol{\varepsilon} + \Delta_{n-1}) + \mu P^t P] \mathbf{f}_n \\ & = [c(H_L(\boldsymbol{\varepsilon} + \Delta_{n-1}))^t c(H_L(\boldsymbol{\varepsilon} + \Delta_{n-1})) + \mu c(P^t P)]^{-1} H_L(\boldsymbol{\varepsilon} + \Delta_{n-1})^t \mathbf{g}. \end{aligned} \quad (1.49)$$

It is noted that when the regularization matrix P is equal to R , the first order difference operator matrix, $c(R^t R) = R^t R$ and the matrix $R^t R$ can be diagonalized by the discrete cosine transform matrix. In [41], it has been shown that the singular values of the preconditioned matrices in (1.49) are clustered around 1 for sufficiently small subpixel displacement errors. Hence when the conjugate gradient method is applied to solve the preconditioned system (1.49), fast convergence is expected. Numerical results in [41] have shown that the cosine transform preconditioners can indeed speed up the convergence of the method.

For each PCG iteration, one needs to compute a matrix-vector product

$$[H_L(\boldsymbol{\varepsilon} + \Delta_n)^t H_L(\boldsymbol{\varepsilon} + \Delta_{n-1}) + \mu R^t R] \mathbf{v}$$

for some vector \mathbf{v} . Since $H_L(\boldsymbol{\varepsilon} + \Delta_n)$ has only $(L+1)^2$ non-zero diagonals and $R^t R$ has at most five nonzero entries in each row, the computational complexity of this matrix-vector product is $O(L^2 M_1 M_2)$. Thus the cost per each PCG iteration is $O(M_1 M_2 \log M_1 M_2 + L^2 M_1 M_2)$ operations. Hence the total cost for finding the solution in (1.45) is $O(M_1 M_2 \log M_1 M_2 + L^2 M_1 M_2)$ operations.

Besides solving the linear system in (1.45), one also needs to solve the least squares problem (1.46) or determine the solution from (1.48). From (1.48), it is noted that one needs to compute

$$Q(\mathbf{f}_n) = [\mathbf{f}_{n\ 00}^y \mid \mathbf{f}_{n\ 00}^x \mid \mathbf{f}_{n\ 01}^y \mid \mathbf{f}_{n\ 01}^x \mid \cdots \mid \mathbf{f}_{n\ L-1L-2}^y \mid \mathbf{f}_{n\ L-1L-2}^x \mid \mathbf{f}_{n\ L-1L-1}^y \mid \mathbf{f}_{n\ L-1L-1}^x]$$

and then solve a $2L^2$ -by- $2L^2$ linear system. Since the matrix-vector product $H_L(\boldsymbol{\varepsilon} + \Delta_n) \mathbf{v}$ for any vector \mathbf{v} can be computed in $O(L^2 M_1 M_2)$ operations, the cost of computing $Q(\mathbf{f}_n)$ is $O(L^4 M_1 M_2)$. The cost of solving the corresponding $2L^2$ -by- $2L^2$ linear system is $O(L^6)$ by using Gaussian elimination. Hence the total cost for finding the solution in (1.46) is $O(L^6 + L^2 M_1 M_2)$ operations.

Finally, it is remarked that L (for instance, the size of the sensor array is equal to 2 or 4) is usually significantly less than M_1 or M_2 (for instance, the size of the image is larger than 256), Hence the total cost for each iteration in the alternating minimization algorithm is approximately $O(M_1 M_2 \log M_1 M_2 + L^2 M_1 M_2)$ operations.

1.7.3 Simulation Results

In the computer simulation, a 256×256 image (Figure 1.10(left)) is taken to be the original high-resolution image. A (2×2) sensor array with sub-pixel displacement errors retrieves four 128×128 blurred and undersampled images, which are corrupted by white Gaussian noise with a SNR of 30 dB. The image interpolated from these low-resolution images is shown in (Figure 1.10(right)). The parameters $\bar{\varepsilon}_{l_1 l_2}^x$ and $\bar{\varepsilon}_{l_1 l_2}^y$ are random values chosen between $\frac{1}{2}$ and $-\frac{1}{2}$.

In the first simulation, the estimated sub-pixel displacement errors, $\varepsilon_{l_1 l_2}^x$ and $\varepsilon_{l_1 l_2}^y$ are set to 85 percent of the real sub-pixel displacement errors. In the proposed RCTLS algorithm, the choice of ‘‘proper’’ regularization parameter, μ is very important. Initially, the proposed RCTLS algorithm was implemented with various

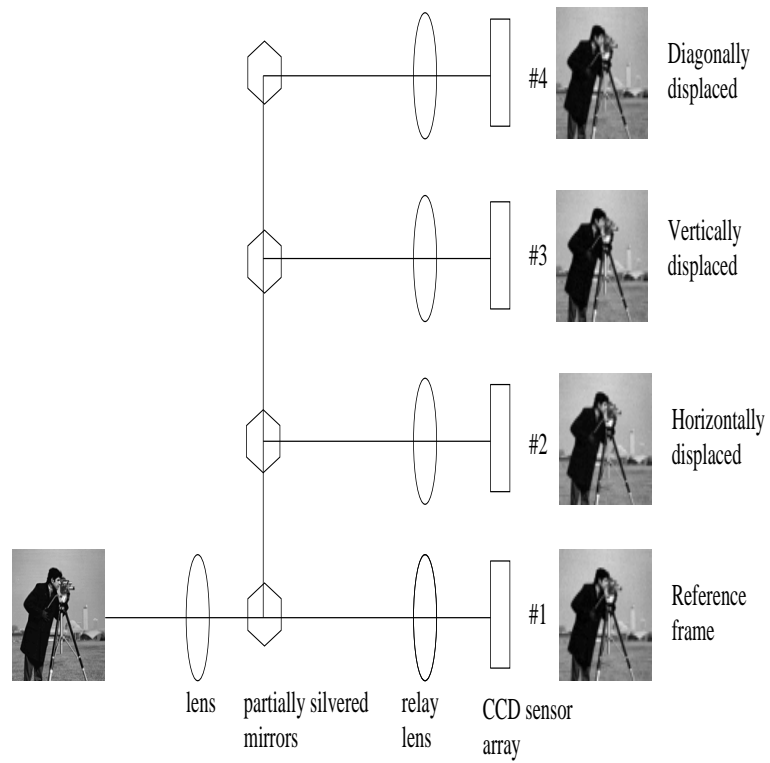


FIGURE 1.9
Example of low-resolution image formation.



FIGURE 1.10
Original image of size 256×256 (left) and observed blurred and noisy image 256×256 ; PSNR=24.20dB (right).



FIGURE 1.11
Reconstructed image by RLS; PSNR = 25.64 dB. (left) and Reconstructed image by RCTLS; PSNR = 25.88 dB (right).

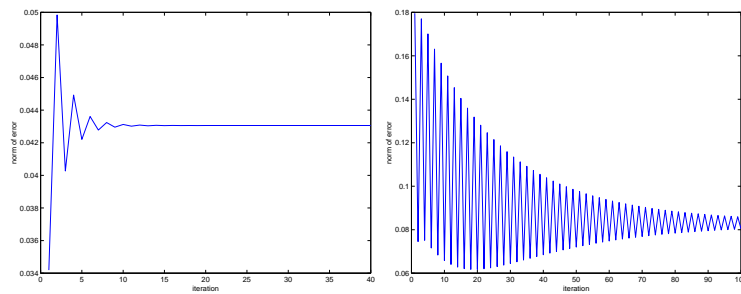


FIGURE 1.12
 Norm of error with $\mu = 10^{-4}$ (left) and norm of error with $\mu = 1$ (right).

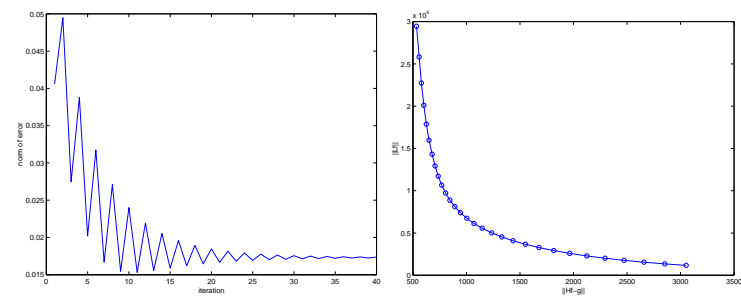


FIGURE 1.13
 Norm of error with $\mu = \mu_{opt}$ (left) and L-curve (right).

values of μ . Define

$$\text{the norm of error at the } n\text{th iteration} = \|\bar{\epsilon} - (\epsilon + \Delta_n)\|_2$$

and plot it for different values of μ (Figures 1.12 and 1.13). The speed of convergence decreases as μ increases. In the case when $\mu = 10^{-4}$ and $\mu = 1$, the norm of error after convergence is greater than that in the first iteration (Figure 1.12). The “inappropriate” value of μ makes the RCTLS solution fall into a local minimum. The L-curve method proposed in [20] may be used to get the optimum value of the regularization parameter. The L-curve method to estimate the “proper” μ for RCTLS was used here. The L-curve plot is shown in Figure 1.13(right). With μ_{opt} retrieved by L-curve, the RCTLS converges to a better minimum point (the norm of error is significantly smaller than those obtained by choosing $\mu = 10^{-4}$ and $\mu = 1$). Table 1.2 shows the estimated subpixel displacement errors by RCTLS with different values of μ . It is seen that the updated subpixel displacement errors with μ_{opt} are closer to the real subpixel displacement errors than the updated subpixel displacement errors with arbitrarily chosen values for regularization parameters μ . It implies better use of the more precise blurring matrix for image reconstruction when the “proper” regularization parameter is chosen.

To show the advantage of the proposed RCTLS algorithm over the conventional RLS (regularized least squares) algorithm, the two methods are compared. The reconstructed image by RLS and the reconstructed image by RCTLS are shown in Figure 1.11(right), respectively. The reconstructed high-resolution image using RCTLS shows improvement both in image quality and PSNR. It is remarked that the optimal regularization parameter for RLS is also determined by L-curve for use in the RLS algorithm.

1.8 Concluding Remarks and Current Work

In summary, we have presented a new approach image restoration by using regularized, constrained total least squares image methods, with Neumann boundary conditions. Numerical results indicate the effectiveness of the method. An application for the approach proposed here is regularized constrained total least squares(RCTLS) reconstruction from a image sequence captured by multisensors with subpixel displacement errors that produces a high-resolution output, whose quality is enhanced by a proper choice of the regularization parameter. The novelty of this application lies in the treatment of the nonsymmetric PSF estimation problem arising from the multisensor image acquisition system.

Finally, we mention some ongoing work on the development of high-resolution algorithms and software for array imaging systems. Compact, multi-lens cameras can provide a number of significant advantages over standard single-lens camera systems, but the presence of more than one lens poses a number of difficult problems.

Errors (x-direction)	$\ell_1 = 0, \ell_2 = 0$	$\ell_1 = 1, \ell_2 = 0$	$\ell_1 = 0, \ell_2 = 1$	$\ell_1 = 1, \ell_2 = 1$
$\bar{\varepsilon}_{\ell_1 \ell_2}^x$	0.2	-0.2	0.1	0.1
$\varepsilon_{\ell_1 \ell_2}^x$	-0.17	-0.17	0.085	0.085
$\varepsilon_{\ell_1 \ell_2} + \delta \varepsilon_{\ell_1 \ell_2}^x$ with $\mu = 10^{-4}$	0.1871	-0.1806	0.0915	0.0856
$\varepsilon_{\ell_1 \ell_2} + \delta \varepsilon_{\ell_1 \ell_2}^x$ with $\mu = 1$	0.2343	-0.2218	0.1290	0.1262
$\varepsilon_{\ell_1 \ell_2} + \delta \varepsilon_{\ell_1 \ell_2}^x$ with $\mu_{opt} = 0.005092$	0.1987	-0.1946	0.0967	0.0957

Errors (x-direction)	$\ell_1 = 0, \ell_2 = 0$	$\ell_1 = 1, \ell_2 = 0$	$\ell_1 = 0, \ell_2 = 1$	$\ell_1 = 1, \ell_2 = 1$
$\bar{\varepsilon}_{\ell_1 \ell_2}^y$	0.1	0	-0.3	-0.2
$\varepsilon_{\ell_1 \ell_2}^y$	0.085	0	-0.255	-0.17
$\varepsilon_{\ell_1 \ell_2} + \delta \varepsilon_{\ell_1 \ell_2}^y$ with $\mu = 10^{-4}$	0.0950	-0.0067	-0.2720	-0.1863
$\varepsilon_{\ell_1 \ell_2} + \delta \varepsilon_{\ell_1 \ell_2}^y$ with $\mu = 1$	0.1034	-0.0235	-0.3373	-0.2361
$\varepsilon_{\ell_1 \ell_2} + \delta \varepsilon_{\ell_1 \ell_2}^y$ with $\mu_{opt} = 0.005092$	0.1038	-0.0011	-0.2857	-0.1952

Table 1.2: Estimation errors.

Modern work on the design and testing of array imaging systems began with seminal papers on the TOMBO (Thin Observational Module for Bound Optics) system described by Tanida et al., in [46, 47]. High-resolution reconstruction methods based on interpolation and projection of pixel values were developed by the authors.

In [13], Chan, Lam, Ng, and Mak describe a new super-resolution algorithm and apply it to the reconstruction of a high-resolution image from low-resolution images from a simulated compound eye (array) imaging system. They explore several variations of the imaging system, such as the incorporation of phase masks to extend the depth of focus. Software simulations with a virtual compound-eye camera are used to verify the feasibility of the proposed architecture and its variations. They also report on the tolerance of the virtual camera system to variations of physical parameters, such as optical aberrations.

In [5], the team consisting of Barnard, Chung, van der Gracht, Nagy, Pauca, Plemmons, Prasad, Torgersen, Mathews, Mirotznik and Behrmann investigate the fabrication and use of novel multi-lens imaging systems for iris recognition as part of the PERIODIC (Practical Enhanced-Resolution Integrated Optical-Digital Imaging Camera) project. The authors of [?] use established, conventional techniques to compute registration parameters and leverage appropriate reconstruction of high-resolution images from low-resolution imagery. To verify that the generated high-resolution images have comparable fidelity to those captured by single-lens camera systems they apply the reconstruction methods to iris recognition biometric problems

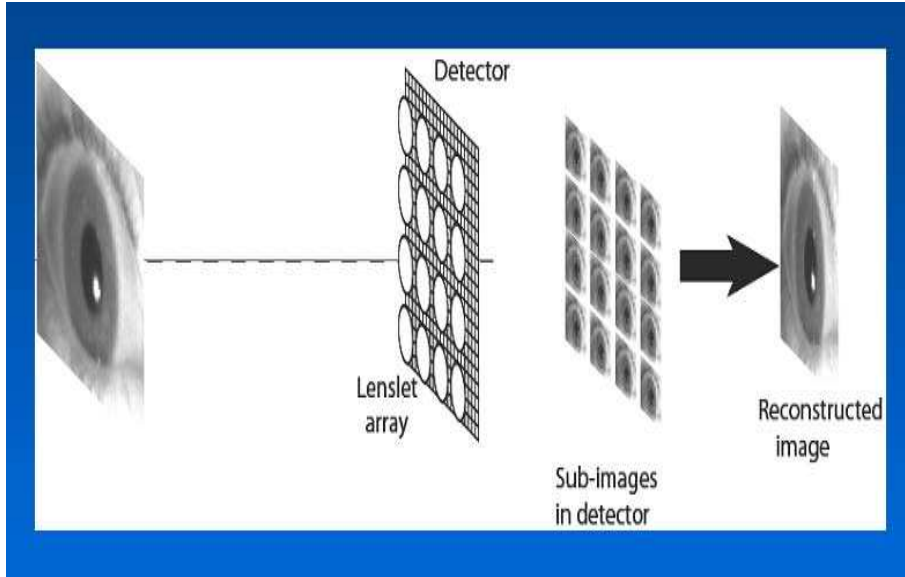


FIGURE 1.14
Lenslet array imaging for biometric identification.

for personnel identification and verification. Figure 1.14 illustrates the collection of an eye image for this biometric application with an array imaging camera.

In [5] the authors also report on image registration and reconstruction results using both simulated and real laboratory multi-lens image data from a prototype array camera fabricated by the PERIODIC research team. Current work on super-resolution construction methods includes not only the use of subpixel displacement methods, but also individual lenslet image diversities such as dynamic range, wavelength and polarization. Array cameras based on novel diffractive lenslets are also being investigated.

Acknowledgments

Research by the first author was supported in part by Hong Kong Research Grants Council Numbers 7046/03P, 7035/04P, 7035/05P and Hong Kong Baptist University FRGs. Research by the second author was supported in part by the Air Force Office of Scientific Research under grant F49620-02-1-0107, by the Army Research Office under grants DAAD19-00-1-0540 and W911NF-05-1-0402, and by ARDA under Contract No. 2364-AR03-A1 through the ORNL.

References

- [1] H. Andrews and B. Hunt, *Digital Image Restoration*, Prentice-Hall, Englewood Cliffs, NJ, 1977.
- [2] O. Axelsson and V. Barker, *Finite Element Solution of Boundary Value Problems, Theory and Computation*, Academic Press, Orlando, FL, 1984.
- [3] M. Banham and A. Katsaggelos, *Digital Image Restoration*, IEEE Signal Processing Magazine, March 1997, pp. 24–41.
- [4] J. Bardsley, S. Jefferies, J. Nagy and R. Plemmons, *A Computational Method for the Restoration of Images with an Unknown, Spatially-varying Blur*, Optics Express, 14, no. 5 (2006), pp. 1767–1782.
- [5] R. Barnard, J. Chung, J. van der Gracht, J. Nagy, P. Pauca, R. Plemmons, S. Prasad, T. Torgersen S. Mathews, M. Mirotznik and G. Behrmann, *High-Resolution Iris Image Reconstruction From Low-Resolution Imagery*, Proceedings of SPIE Annual Conference, Symposium on Advanced Signal Processing Algorithms, Architectures, and Implementations XVI, Vol. 6313, to appear (2006).
- [6] T. Bell, *Electronics and the Stars*, IEEE Spectrum 32, no. 8 (1995), pp. 16–24.
- [7] N. K. Bose and K. J. Boo, *High-resolution Image Reconstruction with Multi-sensors*, International Journal of Imaging Systems and Technology, 9 (1998), pp. 294–304.
- [8] N. K. Bose, H. C. Kim and H. M. Valenzuela, *Recursive Total Least Squares Algorithm for Image Reconstruction from Noisy, Undersampled Frames*, Multidimensional Systems and Signal Processing, 4 (1993), pp. 253–268.
- [9] K. Castleman, *Digital Image Processing*, Prentice-Hall, NJ, 1996.
- [10] R. Chan and M. Ng, *Conjugate Gradient Methods for Toeplitz Systems*, SIAM Review, 38 (1996), pp. 427–482.
- [11] R. Chan, M. Ng and R. Plemmons, *Generalization of Strang’s Preconditioner with Applications to Toeplitz Least Squares Problems*, J. Numer. Linear Algebra Appls., 3 (1996), pp. 45–64.
- [12] T. Chan and C. Wong, *Total Variation Blind Deconvolution*, IEEE Transactions on Image Processing, 7, no. 3 (1998), pp. 370–375.
- [13] W. Chan, E. Lam, M. Ng, G. Mak, *Super-resolution reconstruction in a Computational Compound-eye Imaging System*, Multidimensional Systems and Signal Processing (2006), to appear.
- [14] J. Dennis and R. Schnabel, *Numerical Methods for Unconstrained Optimization and Nonlinear Equation*, Prentice-Hall, 1983.

- [15] H. Engl, M. Hanke and A. Neubauer, *Regularization of Inverse Problems*, Kluwer Academic Publishers, The Netherlands, 1996.
- [16] G. Golub, P. Hansen and D. O’Leary, *Tikhonov Regularization and Total Least Squares*, SCCM Research Report, Stanford, 1998.
- [17] G. Golub and C. Van Loan, *An Analysis of Total Least Squares Problems*, SIAM J. Numer. Anal., 17 (1980), pp. 883–893.
- [18] R. Gonzalez and R. Woods, *Digital Image Processing*, Addison Wesley, New York, 1992.
- [19] M. Hanke and J. Nagy, *Restoration of Atmospherically Blurred Images by Symmetric Indefinite Conjugate Gradient Techniques*, Inverse Problems, 12 (1996), pp. 157–173.
- [20] P. Hansen and D. O’Leary, *The Use of the L-curve in the Regularization of Discrete Ill-posed Problems*, SIAM J. Sci. Comput., 14 (1993), pp. 1487–1503.
- [21] M. Hestenes and E. Steifel, *Methods of Conjugate Gradient for Solving Linear Systems*, J. of Res. Nat. Bureau Standards, 49 (1952), pp.409–436.
- [22] J. Hardy, *Adaptive Optics for Astronomical Telescopes*, Oxford Press, New York, 1998.
- [23] S. Van Huffel and J. Vandewalle, *The Total Least Squares Problem*, SIAM Press, 1991.
- [24] A. Jain, *Fundamentals of Digital Image Processing*, Prentice-Hall, Englewood Cliffs, NJ, 1989.
- [25] S. Jefferies and J. Christou, *Restoration of Astronomical Images by Iterative Blind Deconvolution*, Astrophysics J., 415 (1993), pp. 862–874.
- [26] J. Kamm and J. Nagy, *A Total Least Squares Method for Toeplitz Systems of Equations*, BIT, 38 (1998), pp. 560–582.
- [27] T. Kelley, *Iterative Methods for Optimization*, SIAM Press, 1999.
- [28] D. Kundur and D. Hatzinakos, *Blind Image Deconvolution*, IEEE Signal Processing Magazine, May, 1996, pp. 43–64.
- [29] R. Lagendijk and J. Biemond, *Iterative Identification and Restoration of Images*, Kluwer Academic Publishers, 1991.
- [30] R. Lagendijk, A. Tekalp and J. Biemond, *Maximum Likelihood Image and Blur Identification: a Unifying Approach*, Optical Engineering, 29 (1990), pp. 422–435.
- [31] J. Lim, *Two-dimensional Signal and Image Processing*, Englewood Cliffs, N.J., Prentice Hall, 1990.

- [32] F. Luk and D. Vandevorde, *Reducing boundary distortion in image restoration*, Proc. SPIE 2296, Advanced Signal Processing Algorithms, Architectures and Implementations VI, 1994.
- [33] J. Nelson, *Reinventing the Telescope*, Popular Science, 85 (1995), pp. 57–59.
- [34] V. Mesarović, N. Galatsanos and A. Katsaggelos, *Regularized Constrained Total Least Squares Image Restoration*, IEEE Transactions on Image Processing, 4 (1995), pp. 1096–1108.
- [35] S. Nash and A. Sofer, *Linear and Nonlinear Programming*, The McGraw-Hill Companies, Inc., New York, 1996.
- [36] M. Ng, R. Chan and T. Wang, *A Fast Algorithm for Deblurring Models with Neumann Boundary Conditions*, Res. Rept. 99-04, Dept. Math., The Chinese University of Hong Kong, to appear in SIAM J. Sci. Comput. (1999).
- [37] M. Ng and R. Plemmons, *Fast Recursive Least Squares Using FFT-based Conjugate Gradient Iterations*, SIAM J. Sci. Comput., 17 (1996), pp. 920–941.
- [38] M. Ng, R. Plemmons and F. Pimentel, *A New Approach to Constrained Total Least Squares Image Restoration*, Lin. Alg. and Applic., 316 (2000), pp. 237–258.
- [39] M. K. Ng, R. J. Plemmons and S. Qiao. *Regularized blind deconvolution using recursive inverse filtering*. In G. H. Golub, S. H. Lui, F. T. Luk, and R. J. Plemmons, editors, Proceedings of the Hong Kong Workshop on Scientific Computing, (1997), pp. 110–132.
- [40] M. Ng, R. Plemmons and S. Qiao, *Regularization of RIF Blind Image Deconvolution*, IEEE Transactions on Image Processing, 9, no. 6, (2000), pp. 1130–1134.
- [41] M. Ng and A. Yip, *A Fast MAP Algorithm for High-Resolution Image Reconstruction with Multisensors*, Multidimensional Systems and Signal Processing, 12, 2 (2001), pp. 143–164.
- [42] K. Rao and P. Yip, *Discrete Cosine Transform: Algorithms, Advantages, Applications*, Academic Press, Boston, 1990.
- [43] M. Roggemann and B. Welsh, *Imaging Through Turbulence*, CRC Press, Boca Raton, FL, 1996.
- [44] Y. Saad, *Iterative methods for sparse linear systems*, PWS, Boston, 1996.
- [45] G. Strang, *The Discrete Cosine Transform*, SIAM Review, 41 (1999), pp. 135–147.
- [46] J. Tanida, T. Kumagai, K. Yamada, S. Miyatake, K. Ishida, T. Morimoto, N. Kondou, D. Miyazaki and Y. Ichioka, *Thin Observation Module by Bound Optics (TOMBO): Concept and Experimental Verification*, Appl. Optics, 40 (2001), pp. 1806–1813.

- [47] J. Tanida, R. Shogenji, Y. Kitamura, K. Yamada, M. Miyamoto and S. Miyatake, *Color Imaging with an Integrated Compound Imaging System*, Optics Express, 11 (2003), pp. 2109–2117.
- [48] S. Van Huffel and J. Vandewalle, *The Total Least Squares Problem: Computational Aspects and Analysis*, SIAM Publications, Philadelphia, 1991.
- [49] C. Vogel, T. Chan and R. Plemmons, *Fast Algorithms for Phase Diversity-based Blind Deconvolution*, in Adaptive Optical System Technologies, Proceedings of SPIE, Edited by D. Bonaccini and R. Tyson, 3353 (1998) pp. 994–105.
- [50] Y. You and M. Kaveh, *A Regularization Approach to Joint Blur Identification and Image Restoration*, IEEE Trans. on Image Proc., 5 (1996), pp. 416–427.
- [51] W. Zhu, Y. Wang, Y. Yao, J. Chang, H. Graber and R. Barbour, *Iterative Total Least Squares Image Reconstruction Algorithm for Optical Tomography by the Conjugate Gradient Algorithm*, J. Opt. Soc. Amer. A, 14 (1997), pp. 799–807.
- [52] W. Zhu, Y. Wang, and J. Zhang, *Total Least Squares Reconstruction with Wavelets for Optical Tomography*, J. Opt. Soc. Amer. A, 15 (1997), pp. 2639–2650.